Sediment routing systems of the eastern red sea rifted margin

Guillaume Baby, Antoine Delaunay, Delphine Rouby, Jing Ye, Tihana Pensa, Abdulkader M Afifi

Earth-Science Reviews 249 (2024) 104679

Contents lists available at ScienceDirect

Earth-Science Reviews

journal homepage: www.elsevier.com/locate/earscirev

Sediment routing systems of the eastern red sea rifted margin

Guillaume Baby [a,*], Antoine Delaunay [a], Delphine Rouby [b], Jing Ye [a], Tihana Pensa [a], Abdulkader M. Afifi [a]

[a] Physical Science and Engineering Division, King Abdullah University of Science and Technology, Thuwal, Saudi Arabia
[b] Géoscience Environnement Toulouse (GET), Université de Toulouse, CNRS, IRD, UPS, CNES, F31400 Toulouse, France

ARTICLE INFO

Keywords:
Red Sea
Stratigraphy
Paleogeography
Sediment budget
Source-to-sink

ABSTRACT

We investigate the sediment routing systems of the eastern Red Sea rifted margin by constraining the sediment accumulation history of the offshore depositional domain from regional seismic sections, wells, and outcrops observations and comparing it to the denudation history of the onshore erosional domain (Arabian Shield - Delaunay et al. (2024, submitted in this issue). We show that the rift (28–16 Ma) was segmented into a northern high-relief segment (28°N-21.5°N) under marine depositional environments and a southern low-relief magmatic segment (21.5°N-13°N) under continental depositional environments. The late *syn*-rift (Transition period - 16-14 Ma) was associated with a decrease in the magmatic and tectonic activity of the rifted margins, marine flooding of the entire basin, and the onset of the evaporitic sequence resulting from partial isolation from the global ocean. During the early post-rift (14–5 Ma), the southern segment underwent an uplift and a significant increase of the siliciclastic accumulation (15 fold), suggesting a rapid retreat of the escarpment initially corresponding to the former rift shoulder. During the late post-rift (5–0 Ma) the siliciclastic accumulation dropped and carbonate sedimentation returned suggesting a shift towards arid climatic conditions and a slowdown in the retreat of the onshore escarpment.

1. Introduction

The onshore morphology on many rifted margins is characterized by great escarpments, corresponding to 1000–2500 m topographic steps, sub-parallel to the coast, that separate the low relief higher plateau from the lower rugged coastal plain. This type of morphology is commonly considered to be sustained by the flexural isostatic rebound associated with the erosion of an escarpment allowing the persistence of the regional drainage divides through geological times (e.g., Braun and Beaumont, 1989; Gilchrist and Summerfield, 1990; Kooi and Beaumont, 1994; Tucker and Slingerland, 1994). The remaining key questions related to this topic include the timing of the plateau uplift (i.e. pre-dating, concomitant, postdating the rifting); and the relative contribution of external factors (e.g., climate) on the rate and type of escarpment evolution.

Studies combining numerical modeling with thermochronological constraints suggest *syn*-rift vertical motions can explain the high-elevated margin morphology (e.g., van der Beek et al., 1994; van der Beek et al., 2002). On the other hand, studies based on offshore stratigraphic observations revealed short-lived post-rift uplifts implying significant rejuvenation of margin reliefs and drainage reorganization (e.g., Baby et al., 2018; Burke and Gunnell, 2008; Japsen et al., 2006). One of the best-documented examples is the rifted margins of southern Africa, where the present-day topography of the South African plateau appears to have been acquired by mantle dynamics support, over 40 Myr after the end of the South Atlantic rift (Baby et al., 2020; Braun et al., 2014; Stanley et al., 2021). By comparison, climatic control on the evolution of rifted margin reliefs (i.e. feedback between orographic precipitations and erosional unloading) has received less attention (e.g., Partridge, 1997; Petit et al., 2007; Sternai et al., 2021; Stuwe et al., 2022).

To gain further insights into the evolution of the relief of rifted continental margins at geological time scale, we study the Red Sea, one of the youngest rifted margins on the planet (~28–0 Ma). Recent studies have shown that the Red Sea is mainly floored by oceanic crust accreted since ~14–13 Myr (e.g., Augustin et al., 2021; Delaunay et al., 2023; Tapponnier et al., 2013). We study the eastern rifted margin showing an escarpment that separates the Arabian Plateau from the Red Sea coastal plain. This escarpment is twice as high in the south than in the north (i.e. mean elevation ~2000 m and ~ 1000 m respectively) (Fig. 1).

* Corresponding author.
E-mail address: baby.guillaume@gmail.com (G. Baby).

https://doi.org/10.1016/j.earscirev.2024.104679
Received 25 June 2023; Received in revised form 13 December 2023; Accepted 12 January 2024
Available online 13 January 2024

Remnant marine sediments scattered across the Arabian Plateau indicate that it was at sea level during the Eocene (e.g., Ziegler, 2001). A regional Oligocene angular unconformity indicates a regional uplift of the Nubian-Arabian plateau at the onset of rifting (i.e. Afro-Arabian Dome - Avni et al., 2012). Numerical models from van der Beek et al. (1995) constrained by thermochronological data suggest that the relief of the eastern rifted margin results from a local base-level fall during the rifting followed by continuous retreat of the rift shoulder. Stuwe et al. (2022) and Turab et al. (2023) proposed, from new thermochronological data, an additional uplift of the margin at the onset of the oceanic crust accretion driven by downward bending of the margin and additional flexural updoming. Stuwe et al. (2022) also invoke climate currently

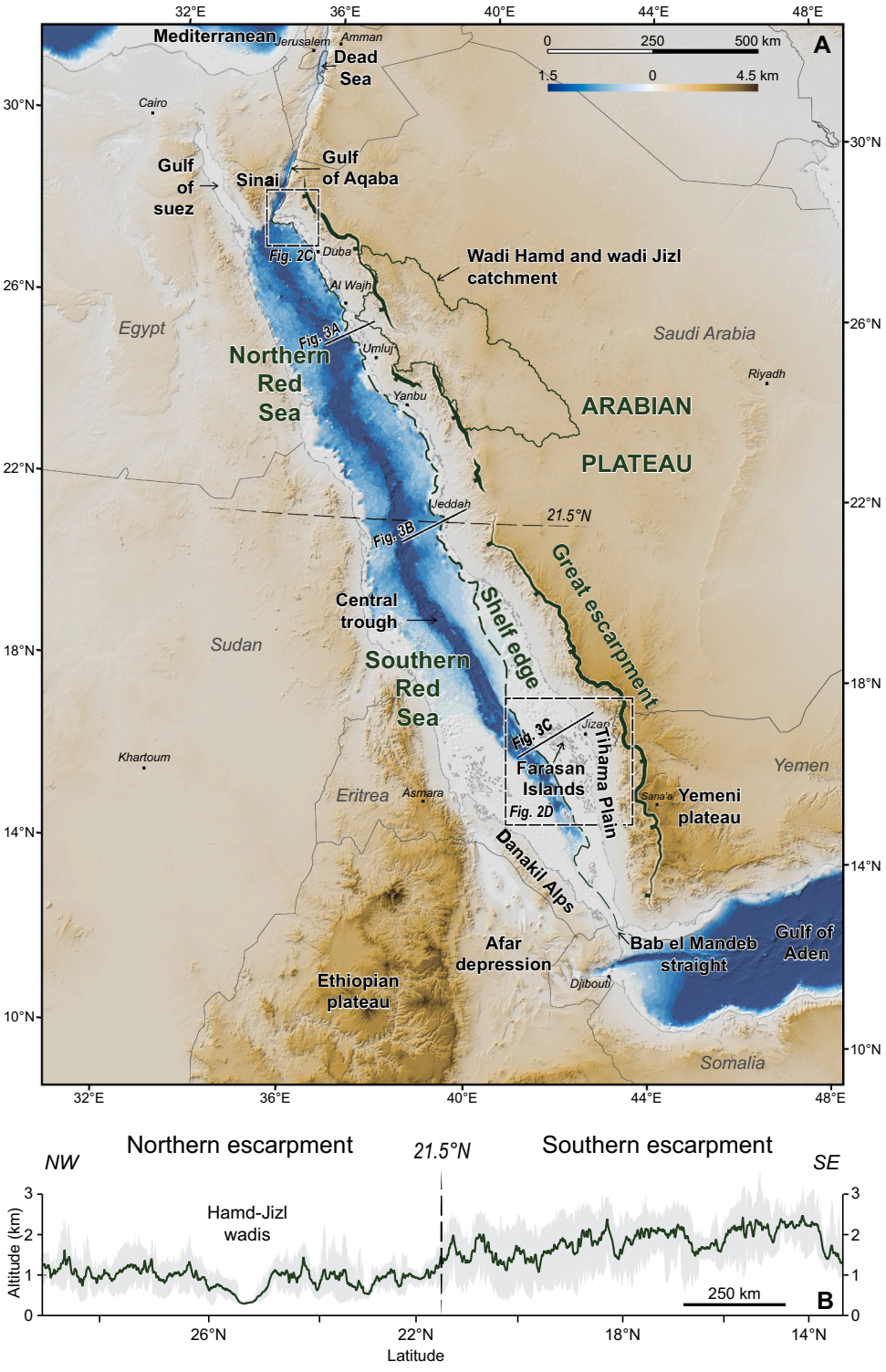

Fig. 1. (A) Regional map of the Red Sea and its surroundings illustrating the main morphological domains of the ERSRM. Elevation data are from GEBCO (https://www.gebco.net/). (B) Maximum, minimum (gray), and mean elevation (dark green line) of the great escarpment of the ERSRM along a 20 km swath. Note the elevation change at 21.5°N between the northern escarpment (~1000 m of mean elevation) and the southern escarpment (~2000 m of mean elevation). (For interpretation of the references to colour in this figure legend, the reader is referred to the web version of this article.)

wetter in the south of the Red Sea to explain the contrasting topography of the escarpment.

Baby et al. (2024, submitted) showed that the contrasted topography of the escarpment along the rifted margin is perfectly mirrored offshore in the structural segmentation of the margin (Fig. 2A). The northern segment geometry, where the escarpment elevation is relatively low, is characteristic of a magma-poor rifted margin (i.e. tilted blocks separated by synthetic normal faults). Conversely, the southern segment geometry, where the escarpment elevation is higher, is characteristic of a magma-rich rifted margin (i.e. seaward dipping reflectors -SDR- wedges accommodated by antithetic normal faults) (Fig. 3). These geometries suggest that the rifted margin relief was influenced by contrasted lithospheric temperature and strength (i.e. effective elastic thickness).

To constrain the evolution of the escarpments along the Eastern Red Sea rifted margin (ERSRM), we reconstruct the sediment-routing systems that shaped the rifted margin relief since ~28 Ma. We focus on the offshore domain, in particular its stratigraphic architecture, paleogeographic evolution (lithologies and depositional environments) and accumulation histories from the Sinai triple junction to the southern tip of the Red Sea (Fig. 2). To do this we analyze an extensive set of

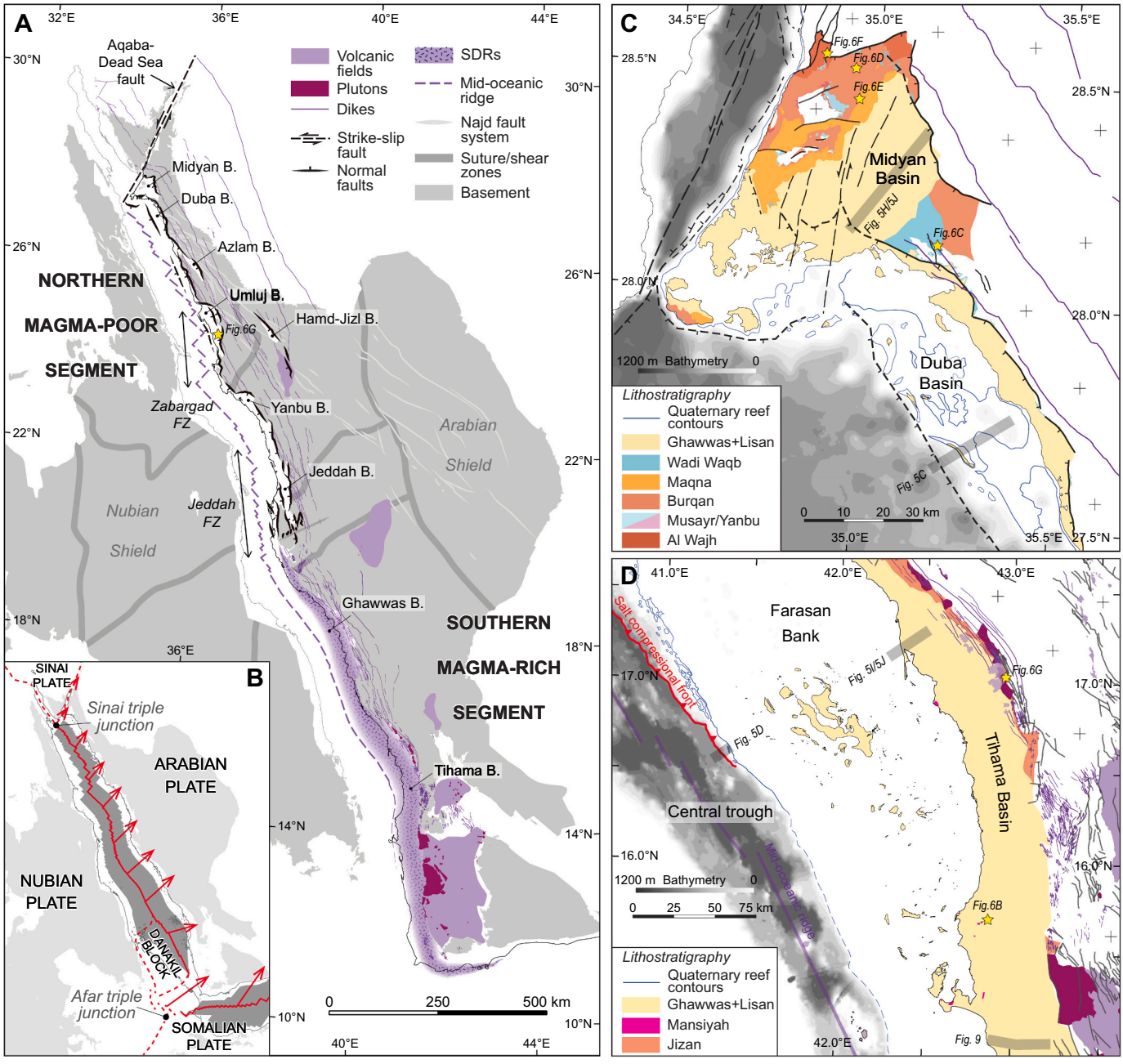

Fig. 2. (A) Syn-rift reconstruction of the Red Sea with major faults, volcanism/magmatism (from Baby et al. (2024, submitted)), and names of coastal basins along the ERSRM. Neoproterozoic sutures and shear zones from Stern and Johnson (2019). (B) Regional tectonic map of the Red Sea and surrounding regions. GPS velocities (red arrows) from Viltres et al. (2022). Areas floored with oceanic crust (dark gray) from Leroy et al. (2013) in the Gulf of Aden and from (Delaunay et al., 2023) in the Red Sea. (C) Geological map of the Midyan and Duba Basins, from Baby et al. (2024, submitted). See location on Fig. 1. Gulf of Aqaba faults are from Ribot et al. (2021). (D) Geological map of the Tihama Basin (Jizan area), from Baby et al. (2024, submitted). See location on Fig. 1. Offshore bathymetry data after GEBCO (https://www.gebco.net/). Refer to Fig. 4B, and C for the ages of the lithostratigraphic units. (For interpretation of the references to colour in this figure legend, the reader is referred to the web version of this article.)

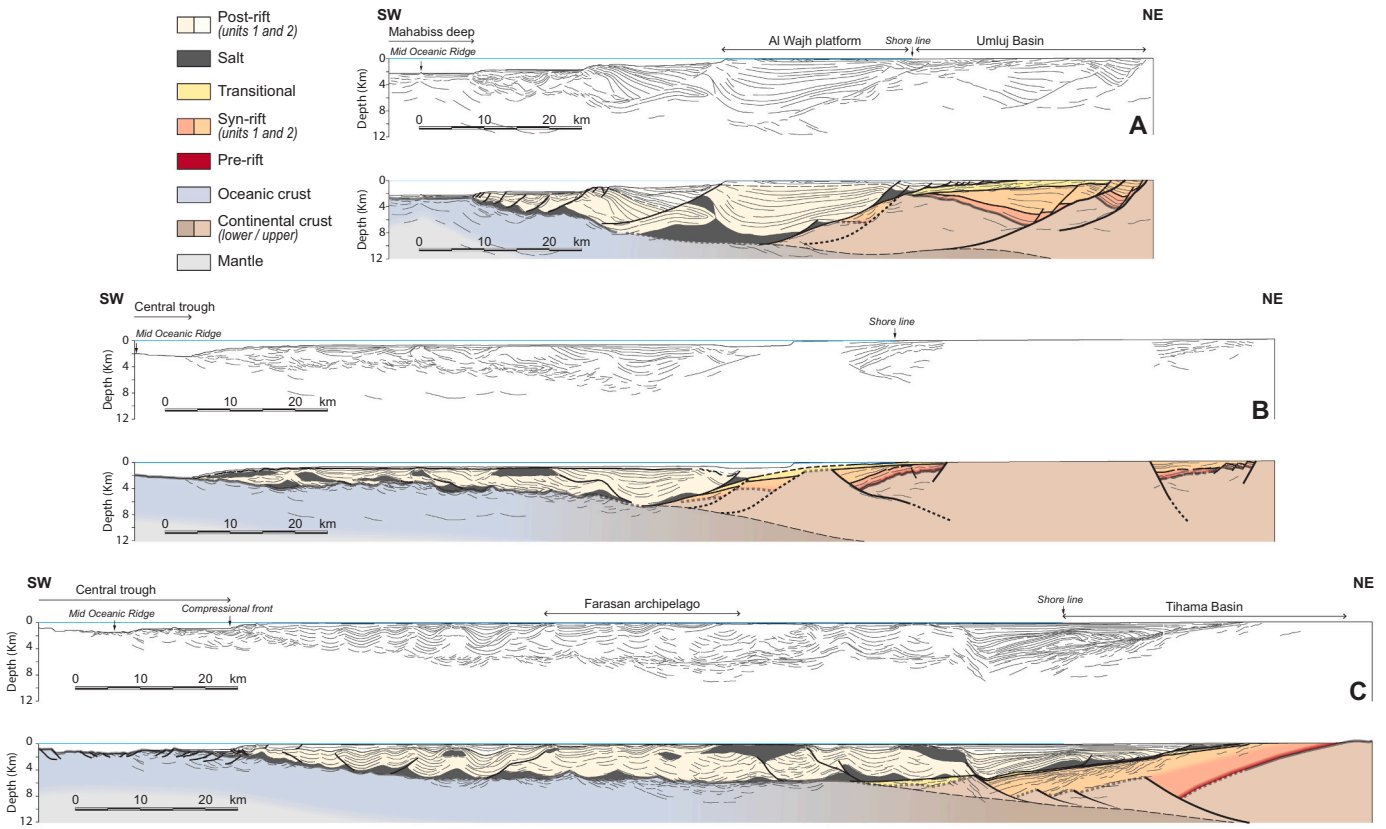

Fig. 3. Line drawings and interpreted cross-sections (from seismic reflection data) across the northern (A), the central (B), and the southern (C) parts of the ERSRM, from the coastal basins to the mid-oceanic ridge. See location on Fig. 1.

subsurface data (seismic and wells) along with outcrop observations. In a companion paper, (Delaunay et al. (2024, submitted in this issue), we focused on the onshore domain and used remnant paleo-landforms of the Arabian Shield to evaluate divides, catchment, and denudation evolution of the source domain of the ERSRM.

2. State of the art

2.1. Tectonic evolution of the Red Sea

The Red Sea rifting was driven by the combination of the far-field slab-pull extension of the subducting Arabian Plate below the Eurasian Plate (Bellahsen et al., 2003) and the lithosphere thermally weakened by the East-Africa hotspot (Vicente de Gouveia et al., 2018). The rifting initiated in the Late Oligocene (~30 Ma) and extended from the Gulf of Suez to the southern Red Sea (Bosworth et al., 2005). Its kinematics was controlled by a pole of rotation located near 38.45°N-25.95°E (Delaunay et al., 2023). The rifting was contemporaneous with continental flood volcanism over northern Ethiopia/Eritrea, northwest Yemen, and southwest Saudi Arabia (Bosworth and Stockli, 2016). Tectonic subsidence in the rifted margin basins increased during the Early Miocene (~24–21 Ma) (e.g., Moretti and Colletta, 1987) along with the denudation along the rifted margins (e.g., Balestrieri et al., 2005; Bohannon et al., 1989; Szymanski et al., 2016). Basaltic dikes, igneous complexes, and a few volcanic fields were emplaced at the time, mainly along the ERSRM (Sebai et al., 1991). During the Middle Miocene (~16–13 Ma), a regional plate reorganization resulted in the abandonment of the Suez Rift, the transfer of motion to the Aqaba-Dead Sea strike-slip fault (Courtillot et al., 1987; Le Pichon and Gaulier, 1988) and the individualization of the Sinai Microplate (Fig. 2A). This induced a shift from normal to oblique extension between the Nubian and Arabian plates, driven by a new pole of rotation around 31.7°N-24.62°E and the onset of seafloor spreading along the full length of the Red Sea (Delaunay et al., 2023). During the late Miocene (~11 Ma), the Danakil Block separated from the Nubian Plate by a counter-clockwise rotation around a pole of rotation located at the tip of the plate, partitioning the extension in the southern Red Sea (McClusky et al., 2010; Reilinger and McClusky, 2011). After ~12 Ma, and mostly during the Plio-Quaternary, the transitional-to-strongly-alkalic Harrat volcanic fields were emplaced in a N-S trend over 1400 km in Saudi Arabia, Jordan, and Syria (Camp and Roobol, 1992).

2.2. The Eastern Red Sea rifted margin

2.2.1. Crustal architecture

Wide angle seismic data (e.g., Egloff et al., 1991; Gaulier et al., 1988; Mooney et al., 1985; Rihm et al., 1991), and teleseismic data (e.g., Ahmed et al., 2013; Al-Damegh et al., 2005; Hansen et al., 2007; Hosny and Nyblade, 2016) can be used to broadly subdivide the Red Sea into three types of crustal domains: an unthinned continental crust with an average thickness of ~35 km, a narrow (~100 km wide) necking domain accommodating the thinning of the continental crust down to 10 km thick or less and an hyper-extended crust, between 4.5 and 7.5 km thick and 150 to ~250 km wide, from North to South (Fig. 3). The nature of the distal crustal domain is still debated with two end member hypotheses: (i) hyper-extended continental crust and/or exhumed continental mantle with the young oceanic crust (<5 Ma) restricted to the axial region in the south (e.g., Ali et al., 2023; Bosworth et al., 2005; Cochran, 2005; Stockli and Bosworth, 2019) and (ii) oceanic lithosphere from north to south formed since ~14–13 Ma (e.g., Augustin et al., 2021; Delaunay et al., 2023; Izzeldin, 1987).

Baby et al. (2024, submitted) show that the necking domain of the ERSRM is segmented between a northern poor-magmatic segment (28°N-21.5°N) with tilted blocks bounded by synthetic normal faults,

and a southern volcanic segment (21.5°N-13°N) showing SDRs wedges accommodated by antithetic normal faults (Figs. 2A and 3). The transition between the two segments is sharp. It is located in the middle of the Red Sea (Baby et al., 2024, submitted), at the latitude of pre-existing onshore lithospheric structures (i.e. Neoproterozoic sutures and shear zones) that played a crucial role in the rift morphology (Molnar et al., 2020). Indeed, these deeply rooted structures, mirrored offshore by the Jeddah Fracture Zone (Fig. 2A), could have controlled the *syn*-rift magma distribution and, in doing so, limited the influence of the East-African hotspot to the southern segment of the rifted margin (Guan et al., 2021).

2.2.2. Lithostratigraphy

The sedimentary record of the margin in Saudi Arabia has been divided into lithostratigraphic units based on surface outcrops and well data (e.g., Al-Shanti, 1966; Dullo et al., 1983; Gillman, 1968; Hughes et al., 1999; Ouf and Gheith, 1998; Schmidt and Hadley, 1985; Schmidt et al., 1983) summarized by Hughes and Johnson (2005) (Fig. 4). The oldest unit of continental clastic sediments (Al Wajh Formation), is locally exposed in the coastal basins of the northern segment of the rifted margin, and the volcanoclastic series of the Jizan Group are well exposed along the Tihama Plain in the southern segment (Fig. 2C and D). This unit has been assigned to the Late Oligocene-Early Miocene based on vertebrate fossils (Schmidt et al., 1983; Zalmout et al., 2010) and radiometric ages of volcanic rocks (Sebai et al., 1991). The first documented marine sediments include the Aquitanian carbonate platform of the Musayr Formation and the evaporites of the Yanbu Formation exposed in the Midyan Basin (Dullo et al., 1983). The later were dated by strontium isotopes from well samples in the Yanbu Basin between 23 and 21 Ma (Hughes and Johnson, 2005). The following Burqan Formation recorded marine clastic sediments (mainly turbidites and debris flows), exposed in the Midyan Basin and in the wells of the Duba Basin (Fig. 2C). The Burqan Formation unit was dated between biozones N5 and N8 (~22–16 Ma) (Hughes and Varol, 2021). Afterwards, three successive evaporite-rich units were deposited unconformably on the previous units and the basement: the Maqna Group composed of clastic, carbonate, and evaporite marine sediments dated between N8 and N9b biozones (~16–14 Ma) (Hughes and Varol, 2021); the Mansiyah Formation composed of massive evaporites (mainly halite), and the Ghawwas Formation composed of continental to transitional clastic sediments interbedded with evaporites and dated between biozones N14 and N18 (Hughes and Johnson, 2005). Recent strontium isotope dating of the Ghawwas Formation has suggested an older age for the onset of its deposition and constrained the Mansiyah evaporite between 14 and 13.2 Ma (Pensa et al., 2023). Above, the unconformable Plio-Pleistocene Lisan Group unit consists of open marine clastic sediments and aggrading carbonate platforms (Fig. 4).

2.2.3. Tectonostratigraphy

The subsurface stratigraphic architecture of the Saudi part of the rifted margin was first described at its northern end, in the Midyan Basin (Tubbs et al., 2014). 3D reflection seismic data from Tubbs et al. (2014) reveal a half-graben structure mainly active during the deposition of the Al Wajh Formation and reactivated in strike-slip during deposition of the Mansiyah Formation evaporites. In the absence of well data, the age of the filling of the half-graben is not well constrained and has been recently reinterpreted as part of the Burqan Formation based on seismic correlations with the offshore Duba Basin (Baby et al., 2024, submitted). Bayer et al. (1988) showed that strike-slip deformation recorded in the Midyan Basin resulted from the initiation of the Aqaba-Dead Sea strike-slip fault system, which was accompanied by an uplift of the western edge of the basin (Fig. 2C).

Along the southern margin, in Yemen, several studies identified the three stages in the rifted margin evolution (Davison et al., 1994; Davison et al., 1998; Doornenbal et al., 1991; Heaton et al., 1995): a *syn*-rift unit *s.s.* affected by basement faults, a transition unit composed of massive evaporites equivalent to the Mansiyah Formation in Saudi Arabia, little or not affected by basement faults, and a post-rift unit. Although poorly constrained, this tectonostratigraphic subdivision challenged the"-mainly rift" end member tectonic model that suggest that the Red Sea is a still-active rift system (Bosworth et al., 2005).

Recently, Baby et al. (2024, submitted) defined six tectonic units for the ERSRM:

(1) The Syn-rift Unit 1 (28–21 Ma) corresponds to the rift initiation and has been interpreted as a "diffuse" deformation phase forming a network of small half-grabens, some of which are preserved on the proximal domains of the northern margins of the Red Sea (Bosworth, 2015). The Azlam and Hamd-Jizl basins (Fig. 3) are possible relics of this initial phase of Red Sea rifting, resulting from the reactivation of the Neoproterozoic Najd fault system (Bosworth, 2015; Szymanski et al., 2016).

(2) The Syn-rift Unit 2 (21–16 Ma) corresponds to the rift climax focusing deformation along the axis of the rifts of the proto-Red Sea and Suez (Fig. 3). In the Gulf of Suez, 60% to 90% of the total tectonic subsidence of the basin was accomplished during this second stage of the rifting (Moretti and Colletta, 1987).

(3) The Transition Unit (16–14 Ma) is marked by a progressive migration of the deformation through the outer necking domain (Baby et al., 2024, submitted) as indicated by a regional unconformity overlain by sag-type geometries in the inner necking domain and persistence of wedging (i.e. growth-strata) in the outer necking domain (Fig. 4).

(4) The Salt Unit (14–13 Ma), little or not affected by basement faults (Fig. 3), marks the onset of the post-rift subsidence in the necking domain and the beginning of the formation of the distal crustal domain (Baby et al., 2024, submitted).

(5) The Post-rift Unit 1 (13–5 Ma) is marked by a homogenization of the stratigraphic architecture of the margin form north to south (Fig. 4). This suggests a similar mechanism driving the tectonic subsidence and accordingly a comparable type of crust throughout the distal domain of the margin (Baby et al., 2024, submitted). This observation is consistent with the "main ocean" end member model (oceanic lithosphere distributed over the entire Red Sea) of e.g., Delaunay et al. (2023) and therefore suggests that accommodation since ~13 Ma was driven at first order by the thermal subsidence of a progressively accreted oceanic crust.

(5) The Post-rift Unit 2 (5–0 Ma) is bounded by a regional unconformity (Fig. 4) known as the Messinian unconformity (Afifi et al., 2014; Mitchell et al., 2021), formerly referred to as the "S reflector" (Phillips and Ross, 1970). This unit is contemporaneous with the oceanic crust exposed along the axial region in the southern Red Sea.

2.2.4. Paleoceanography

The Red Sea is a semi-enclosed basin connected to the Indian Ocean through the strait of Bab el Mandeb (Fig. 1). Pliocene foraminiferal assemblage from the Deep Sea Drilling Project (DSDP) wells in the Red Sea have an Indo-Pacific affinity suggesting a perennial connection between the Red Sea and the Indian Ocean since ~5 Ma (Fleisher, 1974).

Coastal outcrops along the ERSRM indicate continental depositional environments at initiation of the rift and the occurrence of marine depositional environments in the north of the ERSRM during the Aquitanian (23–21 Ma, i.e. Musayr Formation) (Fig. 4). This suggests a connection of the Red Sea with the global ocean through a marine strait to the Neothetys during rifting. This is supported by the Middle Miocene coral faunas of the Egyptian conjugated rifted margin, which show an affinity with Mediterranean faunas without overlap with Indo-Pacific faunas (Perrin et al., 1998). Conversely, based on offshore well data, Hughes and Beydoun (1992) suggested a connection to the open ocean in the south, with a gradual flooding from the Indian Ocean since the Late Oligocene (~28 Ma). In both cases, the connection with the global ocean was restricted from the Middle Miocene to the Pliocene, as indicated by the precipitation of the Red Sea evaporitic sequence from ~16 Ma to ~5 Ma comprising the Maqna Group, and the Mansiyah and

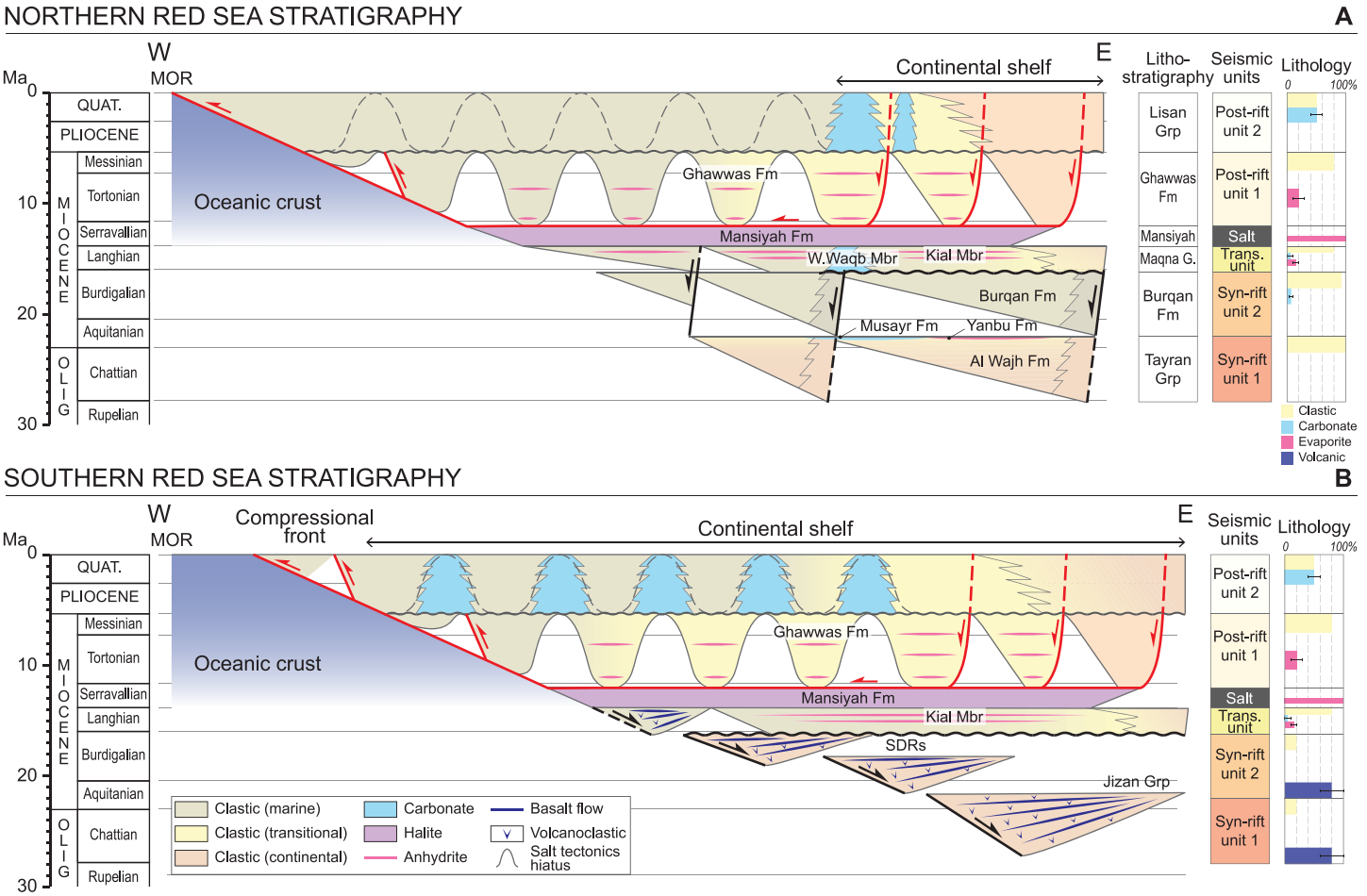

Fig. 4. Simplified Wheeler diagrams showing the east-to-west stratigraphic framework of the northern (A) and southern (B) segments of the ERSRM. The percent lithologies for each tectonostratigraphic units and the lithostratigraphic formations defined by Hughes and Johnson (2005) are also shown.

Ghawwas formations (Fig. 4). Several authors have argued that this paleoenvironmental change was linked to the regional plate reorganization in the Middle Miocene (see above). The activation of the Aqaba-Dead Sea strike-slip fault system would have slightly uplifted the northern part of the Gulf of Suez and significantly reduced the northern connection with the Neothetys (e.g., Bosworth et al., 2005; Perrin et al., 1998).

2.2.5. Relief and drainage of the ERSRM

The onshore morphology of the ERSRM is typical of an elevated rifted margin, with an escarpment delimiting a dissected low coastal plain from a high-elevation plateau gently tilted to the east (landward). Along the north segment (north of 21.5°N), the escarpment ("Arabian Escarpment") is discontinuous with a mean relief of ~1000 m. Along the southern segment (south of 21.5°N), the escarpment is steep and continuous with a mean relief of ~2000 m (e.g., Delaunay et al., 2024, submitted in this issue). The ERSRM is drained by (1) relatively linear rivers crossing the coastal domain from headwaters in the Arabian Escarpment region as well as (2) the catchment of the Hamd and Jizl wadis draining a portion of the plateau (Fig. 1). The offshore bathymetry is segmented as well between the southern and northern ERSRM. The continental shelf is narrow (25–50 km) north of 20°N and widens (100–150 km) to the south, where oceanic crust is exposed in the central trough (Figs. 1 and 2D).

2.2.6. Denudation history of the ERSRM from thermochronology

Apatite fission track (AFT) and (U—Th)/He data are relatively scarce along the rifted margin and mostly limited to the southern segment (Bohannon et al., 1989; Menzies et al., 1992; Menzies et al., 1997; Turab et al., 2023), with the exception of the study by Szymanski et al. (2016) at the latitude of the Umluj Basin (Fig. 2A). All of these studies highlight a period of accelerated denudation at ~25–20 Ma, i.e. coeval of the rifting. In the southern segment, denudation was mainly confined to the ~75 km wide coastal plain, while it affected a ~ 150 km wide area in the northern segment (Szymanski et al., 2016) by reactivation of the Neo-Proterozoic Najd fault system (Stern, 1985) and formation of the Azlam and Hamd-Jizl rift basins (Figs. 2A). Assuming a geothermal gradient of 30–40 °C/km, the average total denudation along the northern segment was about 1.5–2 km (Szymanski et al., 2016). In contrast, assuming a geothermal gradient of 22 °C/km, Bohannon et al. (1989) estimated a total denudation of 3–4 km along the southern segment. Turab et al. (2023) suggested a second stage of denudation of the southern segment at ~13 Ma that they related to the onset of oceanic crust accretion.

2.2.7. Denudation history of the ERSRM from geomorphic mapping

Delaunay et al. (2024, submitted in this issue) mapped and dated the onshore remnant landforms and planation surfaces of the ERSRM. They showed that pre- and *syn*-rift landforms are only preserved on the elevated Arabian Plateau, indicating minimal erosion of the plateau since the Lower Miocene. Erosion of the Red Sea coastal plain started at ~16 Ma when tectonic activity slowed. This allowed the retreat of the escarpment along the northern segment, resulting in the capture of the Hamd-Jizl Basin, and the formation of an important watershed (Fig. 1). The erosion of the coastal plain in the southern segment was more complex. It started with downward erosion before rapidly shifting to scarp retreat erosion driven by the flexural response to denudation. They estimated that the rate of vertical erosion since ~16 Ma was around 5 m/Myr on the Arabian Plateau and 40 mm/Myr on the coastal plain. Along the northern segment, where paleo-landforms are better preserved in the coastal plain, the rate of vertical erosion has been better defined. It was ~60 m/Myr between ~16 to ~5 Ma and dropped to ~5 m/Myr afterwards (Delaunay et al., 2024, submitted in this issue).

3. Data and method

3.1. Data set

To establish the stratigraphic architecture of the ERSRM basins, we interpreted a dense grid of proprietary seismic reflection profiles (spacing ~30–50 km) and extending from the coastal basins to the mid-oceanic ridge (total length ~ 11,000 km). We used 84 exploration wells (located onshore and offshore mainly in the shelf domain), 61 shallow wells (located onshore), and outcrops for calibration of geometries and sedimentary facies.

3.2. Stratigraphic framework

We used the tectonostratigraphic framework of Baby et al. (2024, submitted), who defined six seismic units along the rifted margin (see section 2.2.3, Fig. 4). These include two syn-rift units corresponding to the initiation (Syn-Rift Unit 1) and the climax (Syn-Rift Unit 2) of crustal thinning in the necking domain, a transition unit (Transition Unit) sealing the syn-rift structures in the proximal necking domain while crustal thinning migrated to the distal part of the margin, a thick layer of massive evaporites (Salt Unit) marking the onset of post-rift subsidence, and two post-rift units (Post-Rift Unit 1 and Post-Rift Unit 2) separated by the Messinian unconformity. We reconstructed the depositional environments from the seismic stratigraphy interpretations (Fig. 5), well data and outcrop observations (Fig. 6). To analyze facies variations along the strike of the margin, we correlated the interpreted sedimentary units along a north-south transect of wells and outcrops **(Fig. S1)**.

3.3. Paleoenvironmental maps

From the exploration wells, coastal shallow wells, and outcrop data along the ERSRM, we constructed four depositional environment maps (Fig. 7). Continental environments include fluvial and lacustrine facies, transitional environments include coastal and deltaic plain facies, as well as carbonate platforms, shallow marine environments include continental platform facies (<200 m), and deep marine environments include abyssal facies (>200 m).

3.4. Accumulated volumes and rates of siliciclastic sediments

To determine the volumes and accumulation rates of siliciclastic sediments preserved within each tectonostratigraphic unit, we constructed regional geological cross-sections for the whole depositional area by combining regional seismic sections calibrated in age and lithology. We depth-converted the cross-sections using a multi-layered velocity model. Examples of detailed line drawing of geological cross sections are shown in Fig. 3. **Fig. S2** shows all the sections constructed. We used the method of Baby et al. (2020); Guillocheau et al. (2012); Rouby et al. (2009) to estimate the accumulated volumes and accumulation rates during each time-step from a linear interpolation between sections (Fig. 8 **and Table 1**). We also used the method of Guillocheau et al. (2012) and Rouby et al. (2009) to estimate the associated combined variability related to uncertainties on the (a) depth conversion parameters, (b) calibration in absolute ages of the interpreted stratigraphic horizons, the corrections for (c) in-situ content as opposed to siliciclastic content (i.e. carbonates, evaporites, and volcanism) and (d) remaining porosity. Details of the approach and the uncertainty estimation can be found in Supplementary Section S3.

4. Results

4.1. Sediment accumulation history of the ERSRM

4.1.1. Early rifting (28–22 Ma) – Syn-rift unit 1

Along the northern segment, the earliest tectonic evidences are

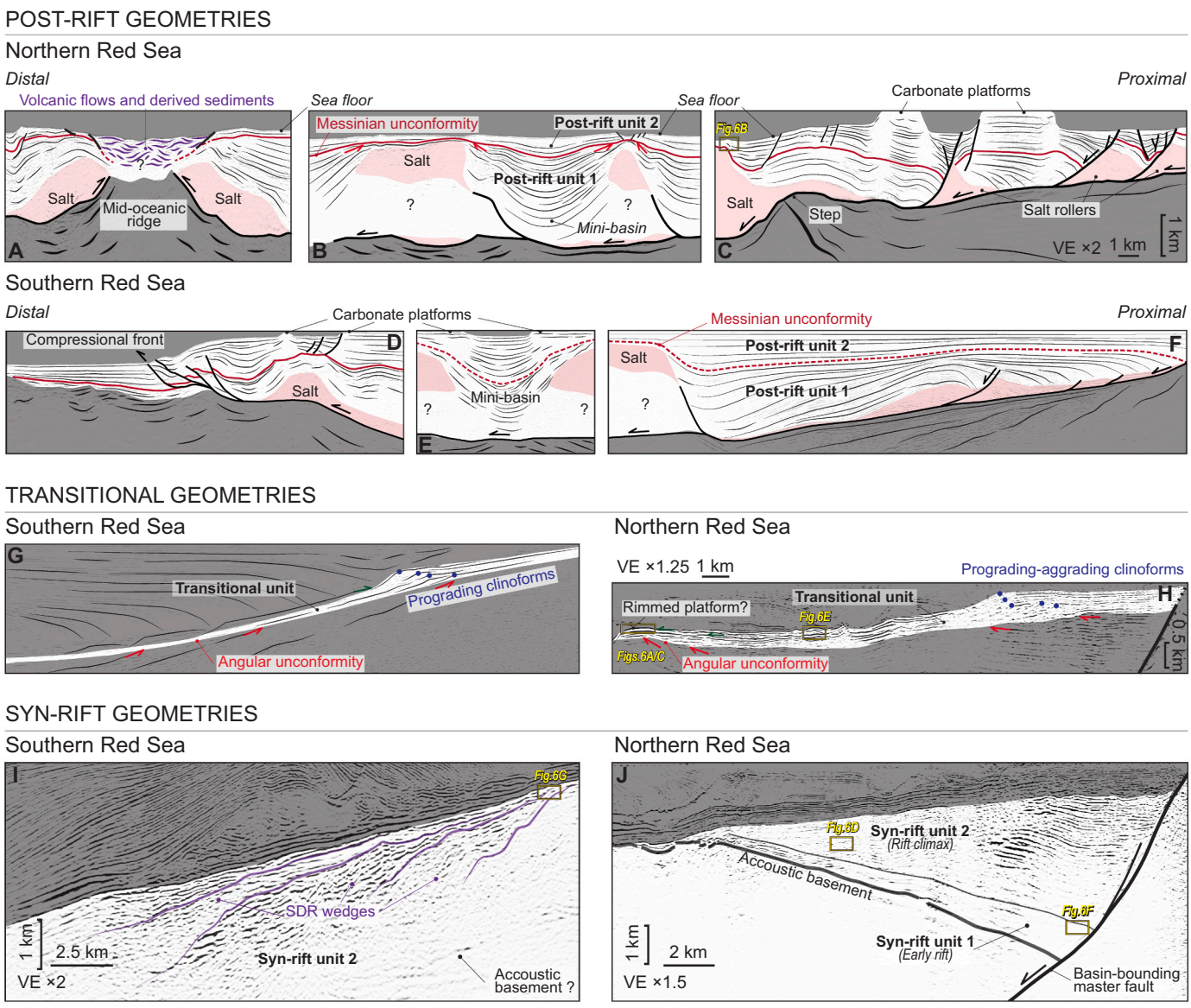

Fig. 5. Seismic facies chart illustrating the subsurface sedimentary geometries and structures of the sedimentary infill of the ERSRM. See location on Fig. 2C, and D. Analog outcrop pictures shown in Fig. 6 are located by the yellow boxes. (For interpretation of the references to colour in this figure legend, the reader is referred to the web version of this article.)

sedimentary wedges showing growth structures and thickening towards seaward-dipping normal faults bounding the coastal basins (Figs. 3A, 4A, and 5J). In contrast, along the southern segment, the normal faults and the *syn*-rift strata dip landward (Figs. 3C, and 4B). The nature of the half-graben infill is also different (Fig. 4). Along the northern segment, it is mainly composed of the fluvial deposits of the Al Wajh Formation, which are well exposed in the Midyan Basin (Figs. 2C, and 6F). Along the southern segment, it is composed of lacustrine sediments with interbedded lava flows and pyroclastic/tuffaceous layers. This assemblage forms the Jizan Group which is well-exposed along the Tihama Plain (Figs. 2D, and 6G). These volcanoclastic series have been interpreted as inner SDRs (Baby et al., 2024, submitted) also described in the Yemeni part of the segment (Chauvet et al., 2023), where they conformably overlie the Oligocene Yemeni-Ethiopian traps. The estimated siliciclastic supply rates were low along the entire rifted margin (<1000 km^3/Myr) with ~3884 km^3 of siliciclastic sediments preserved along the northern segment and ~ 4384 km^3 along the southern one (**Table 1 and** Fig. 8).

4.1.2. Rift climax (22–16 Ma) – Syn-rift unit 2

The rifting climax can be identified by an increase in tectonic subsidence rates in the northern segment (Baby et al., 2024, submitted) (Fig. 5J), as well as by an increase in accumulation rates and volumes (~1750 km^3/Myr and ~ 10,450 km^3 respectively) (**Table 1 and** Fig. 8). This acceleration of the tectonic subsidence is associated with a major change in depositional environments (Fig. 4A) driven by a northward flooding of the Red Sea rift (Fig. 7). This is indicated by the deep marine depositional environments in the Midyan, Duba, and Umluj basins with the deposition of marine turbidites of the Burqan Formation (Figs. 6D). To the south, depositional environments shift to transitional (coastal) in the Yanbu Basin, and to continental in the Jeddah Basin (Fig. 7 **and Fig. S1**). The transitional (coastal to alluvial) sediments are barren of fossils and have been attributed to the Oligocene-Early Miocene Al Wajh Formation (Hughes and Johnson, 2005). As the difference, in the southern segment, the accumulation rate increased only marginally (<1000 km^3/Myr; **Table 1 and** Fig. 8), the depositional environments remained unchanged, and the continued emplacement of SDRs indicate a sustained magmatic activity (Fig. 4B, and 5I).

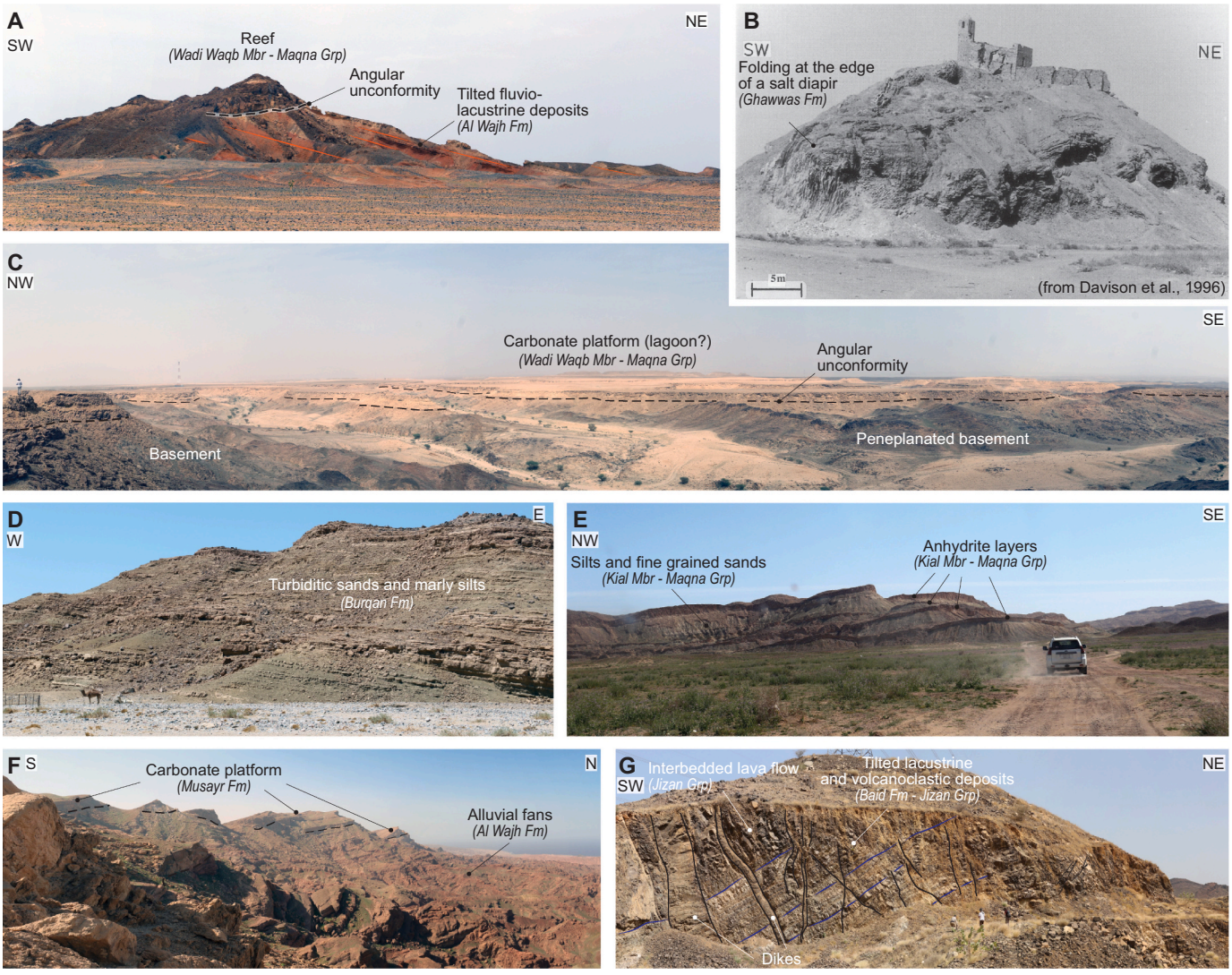

Fig. 6. Field observations illustrating part of the geometries and depositional environments of the ERSRM sedimentary infill. (A) Middle Miocene reef limestones (Wadi Waqb Member) unconformably overlying tilted continental rift sediments (Al Wajh Formation). (B) Northeastern flank of a evaporite diapir deforming Late Miocene transitional (coastal) sediments (Ghawwas Formation). The evaporites are Middle Miocene in age (Mansiyah Formation). Picture after Davison et al. (1996). (C) Middle Miocene carbonate platform (Wadi Waqb Member) unconformably overlying the peneplanated basement at the edge of a tilted bloc. (D) Early to Middle Miocene deep marine sediments (Burqan Formation). (E) Middle Miocene restricted marine sediments with evaporites interbedded within distal marine deposits (Kial Member). (F) Late Oligocene to Early Miocene continental alluvial fans (Al Wajh Formation) unconformably overlained by an Early Miocene carbonate platform (Musayr Formation). (G) Tilted Late Oligocene to Early Miocene continental (lacustrine) deposits (Baid Formation) interbedded with lava flows and tuffaceous sandstones. The whole is intruded by Early Miocene volcanic dikes and forms the Jizan Group. Refer to Fig. 4B, and C for the ages of the lithostratigraphic units. See locations on Fig. 2A, C, and D and corresponding seismic facies on Fig. 5.

4.1.3. *Transition (16–14 Ma) – Transition unit*

The transitional period is marked by a major angular unconformity spanning the entire rifted margin (Fig. 4), sealing the *syn*-rift structures in the proximal necking domain, and indicating a significant deceleration in tectonic and magmatic activity of the rifted margin (Baby et al., 2024, submitted). This unconformity is well imaged along the northern segment, where the Middle Miocene carbonate platforms of the Wadi Waqb Member of the Maqna Group (Hughes, 2014) lie unconformably on the syn-rift deposits and the eroded basement (Fig. 6A, C). Sag-type geometries with deltaic clinoforms in the hanging-wall of the major basin-bounding faults are consistent with a significant decrease in the accommodation available in the basins (Fig. 5H). These deltaic deposits evolve laterally to shelf deposits, which are well exposed in the Midyan Basin and are mainly composed of silts interbedded with evaporites, indicating restricted marine environments (Fig. 6E). These alternating layers of silt and evaporites form the Kial Member of the Maqna Group. The carbonate platforms of the Wadi Waqd Member develop contemporaneously on the crests of the tilted blocks (Fig. 5H) and on the eroded footwall of the basin-bounding faults (Koeshidayatullah et al., 2016; Pensa et al., 2022). Along the southern magmatic segment, geometries and depositional environments are similar to those of the northern segment. They lack however carbonate platforms, which is probably related to the opposite dip of crustal faults that prevented the formation of structural highs in the proximal necking domain and to the high intensity of volcanism, which filled the accommodation available (Fig. 5G). Overall, this period marks the first complete flooding of the Red Sea, with marine environments identified along the entire rifted margin (Fig. 7). The siliciclastic accumulation rates slowed down, along with the tectonic and magmatic activity (**Table 1 and** Fig. 8).

4.1.4. *Early post-rift (14–5 Ma) – Salt unit and Post-rift unit 1*

The early post-rift infill is thick (>2 km), with a massive layer of evaporites (mainly halite) across the rifted margin known in Saudi Arabia as the Mansiyah Formation (Fig. 4). By analogy with other giant

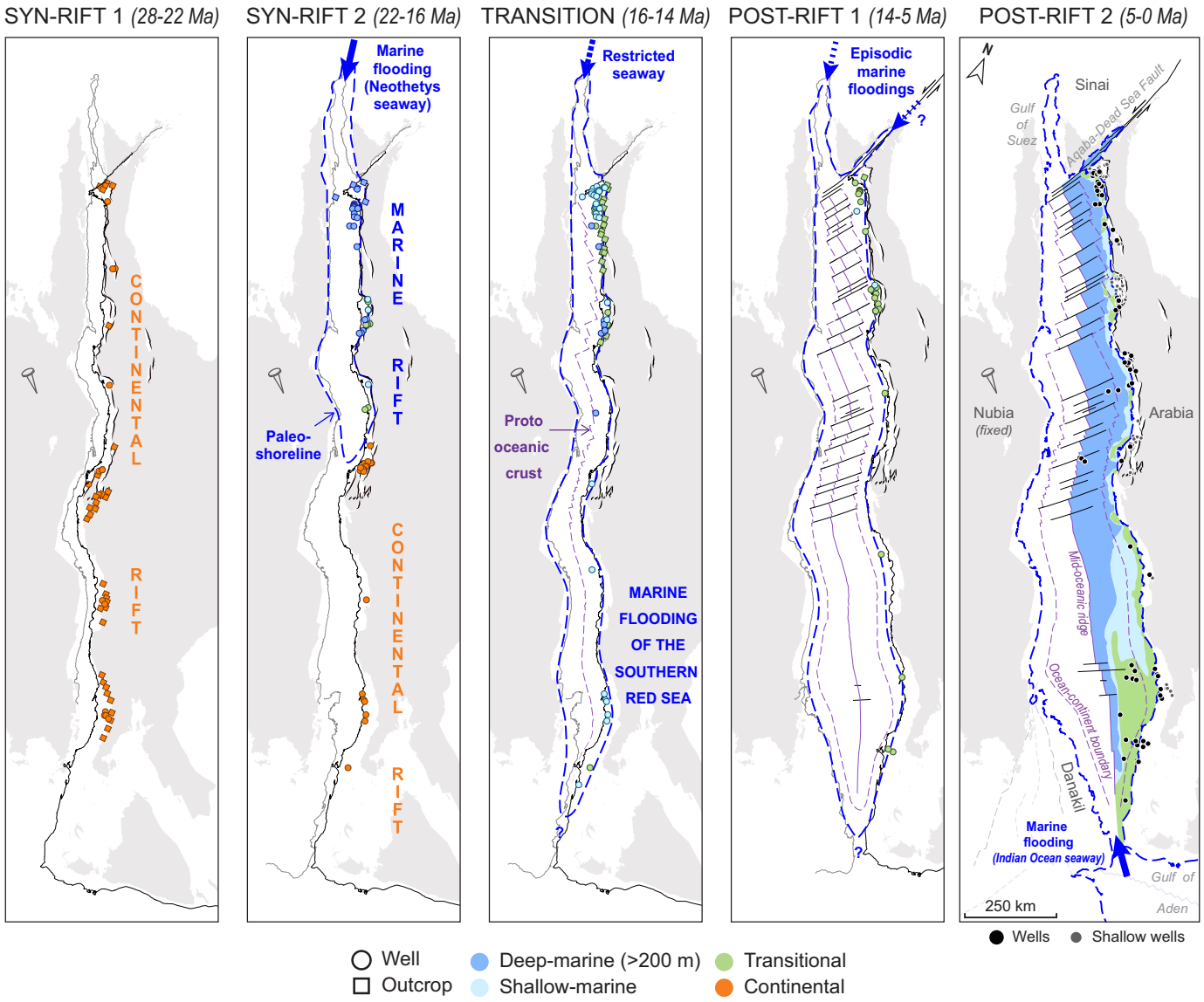

Fig. 7. Paleoenvironmental maps of the ERSRM based on outcrops and well data, superimposed on a palinspastic restoration of the Arabian Plate and Danakil Block. The Nubian Plate is considered as the fixed plate in these reconstructions. The eularian poles are from Delaunay et al. (2023) (Arabian Plate) and McClusky et al. (2010) (Danakil Block). Refer to Fig. 2B for the location and name of the plates.

salt provinces like the Gulf of Mexico (e.g., Pindell et al., 2014) or the South Atlantic (e.g., Chaboureau et al., 2013; Laspatzis et al., 2023), it is likely that it precipitated in <1 Myr, contemporaneously with the first oceanic crust accretion. Recent strontium dating of the evaporites from well samples support this hypothesis (ages from 14 Ma to 13.5 Ma) (Pensa et al., 2023). These evaporites were remobilized and controlled the second-order geometries of the post-rift infill (Fig. 4) with an extensional domain made of salt rollers (Fig. 5C and F), a canopy/extensional diapir domain (Fig. 5B and E), and a compressional domain (Fig. 5A and D). The Mansiyah Formation is not exposed except in small diapirs along the Tihama coastal plain (Fig. 6B). The post-salt Miocene infill of the Ghawwas Formation consists mainly of clastic transitional (coastal) to shallow marine sediments interbedded with evaporites (Figs. 4 **and S1**). The siliciclastic accumulation rates and volumes increased significantly at the time on both segments of the margin (~20,000 km^3/Myr; ~200,000 km^3 in each segment) (**Table 1 and** Fig. 8).

4.1.5. *Late post-rift (5–0 Ma) – Post-rift unit 2*

The late post-rift period begins with the Messinian unconformity (Fig. 4) followed by carbonate deposition with the aggrading platforms along the edge of the shelf. Along the northern segment, the platforms are restricted to the proximal necking domain, growing above the topography inherited from the tilted blocks (Fig. 2C, and 5C). In contrast, along the southern segment, carbonate platforms developed over the entire shelf and down to the edge of the central trench where oceanic crust was exposed (Figs. 2D, 5D, and E). The siliciclastic accumulation decreased significantly during this time interval with a total of ~50,000 km^3 of siliciclastic sediments deposited whole of the rifted margin (**Table 1 and** Fig. 8).

4.2. *Evidence for post-rift uplift of the southern segment of the ERSRM*

Along the onshore part of the southern segment on the Tihama Plain, syn-rift deposits dip seaward with an average of 25–30° (Bohannon et al., 1989; Chauvet et al., 2023; Fedorik et al., 2023; Schmidt and Hadley, 1985; Schmidt et al., 1983). Paleomagnetic data on the dikes that intrude this volcanoclastic sediments and volcanic flows (Kellogg and Blank, 1982) confirm a tilt of ~20° of the coastal plain towards the Red Sea after their emplacement at 24–21 Ma (Sebai et al., 1991).

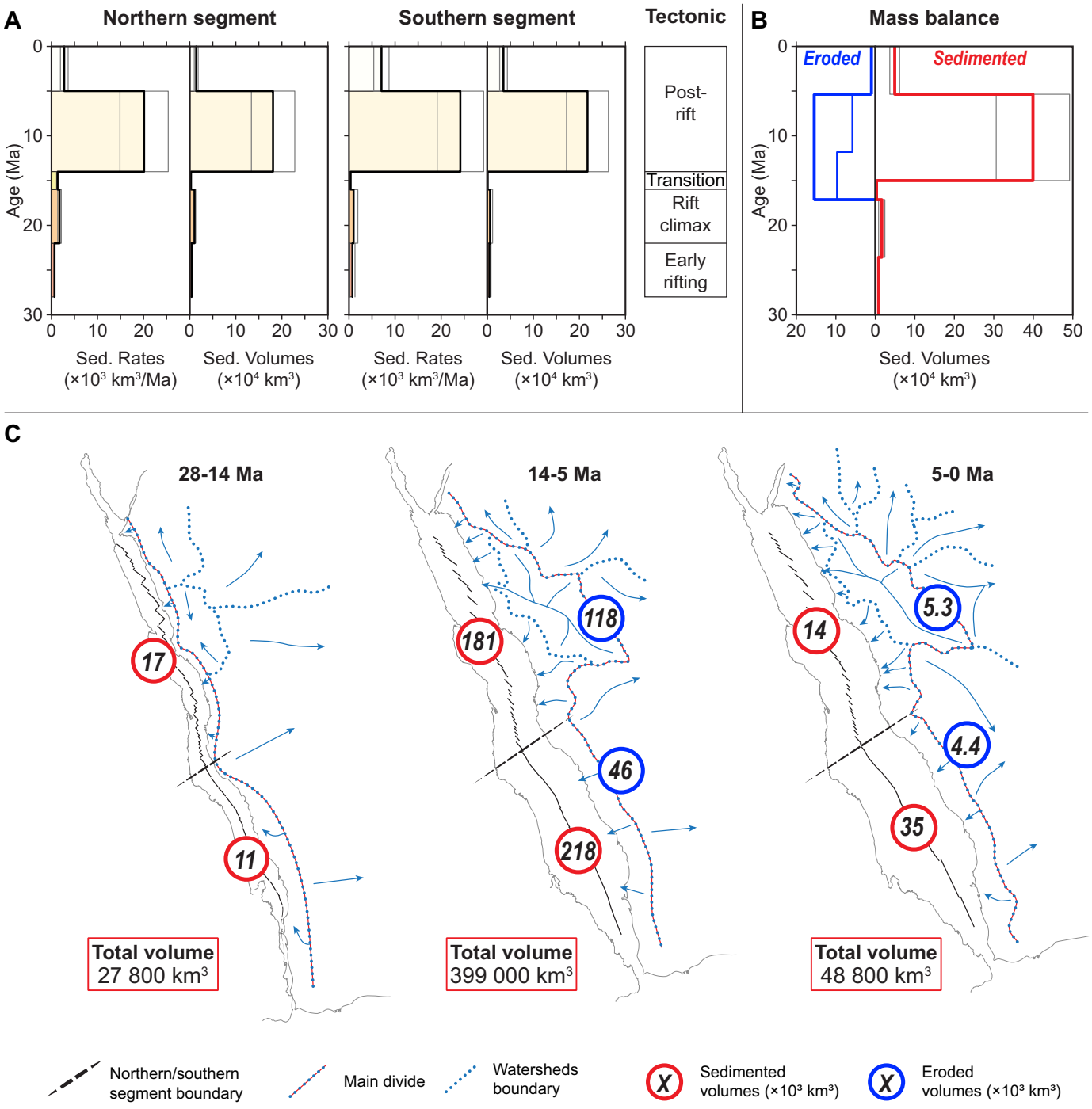

Fig. 8. (A) Accumulated siliciclastic sediment volumes and rates of the northern and southern segments of the ERSRM. Variances (fine lines) correspond to the uncertainties on horizon age, carbonate/salt/volcanic content, and sand/shale ratio. (B) Comparison of the offshore sedimented volumes and of the onshore eroded volumes for the whole margin. (C) Schematic sediment routing system and sediment budget for the *syn*-rift (28–14 Ma), early post-rift (14–5 Ma), and late post-rift (5–0 Ma) periods. Eroded volumes and onshore drainage patterns from Delaunay et al. (2024, submitted in this issue).

Subsurface data support a westward tilting of the margin associated with an angular unconformity clearly cross-cutting the syn-rift strata (inner SDRs) and deltaic clinoforms of the Transitional unit (Fig. 9). Furthermore, this unconformity is onlapped by the Post-rift unit 2, indicating that this margin deformation is a post-rift event that took place between ~14 and ~ 5 Ma. Seismic data available from Saudi Arabia (this study) and Yemen (Davison et al., 1994; Davison et al., 1998; Doornenbal et al., 1991; Heaton et al., 1995) indicate that this tilting affected the entire southern segment of the ERSRM. Post-rift sediments are condensed in the proximal part of the basin and strongly remobilized by salt tectonics, making it difficult to accurately date this tilting (Fig. 9). A recent study based on thermochronological data on the inboard Arabian Escarpment detects an acceleration of denudation at ~13 Ma (Turab et al., 2023) that could be contemporary with the westward tilt of the coastal plain and the offshore deposition of the Mansiyah Formation (Salt unit).

Table 1
Accumulated solid sediment volumes, rates, and associated variance for the ERSRM.

Accumulated siliciclastic volumes, rates and associated variance for the northern segment of the ERSRM					
Tectonic stages	(Ma)	Volume ($\times 10^3$ Km^3)	σ	Rate ($\times 10^3$ Km/Myr)	σ
Late post rift	0–5	13.90	4.20	2.80	0.80
Early post rift	14–5	180.90	47.20	20.10	5.20
Transition	16–14	2.60	0.40	1.30	0.20
Rift climax	22–14	10.50	2.30	1.70	0.40
Early rift	28–22	3.90	0.50	0.60	0.10
Accumulated solid volumes, rates and associated variance for the southern segment of the ERSRM					
Tectonic stages	(Ma)	Volume ($\times 10^3$ Km^3)	σ	Rate ($\times 10^3$ Km/Myr)	σ
Late post rift	0–5	35.10	8.30	7.00	1.60
Early post rift	14–5	217.60	45.50	24.20	5.10
Transition	16–14	0.60	0.10	0.30	0.10
Rift climax	22–14	5.80	5.60	1.00	0.90
Early rift	28–22	4.40	3.40	0.70	0.60

5. Discussion

5.1. Sediment budget

The accumulation history shows a fifteen-fold increase of accumulated volumes of siliciclastic sediments during the post-rift interval (13–0 Ma) compared to the syn-rift interval (28–13 Ma) (Fig. 8A). Also accumulated volumes and accumulation rates decrease significantly in the Pliocene and Quaternary (5–0 Ma) along with the re-establishment of carbonate platforms. Independent estimations of denudation of the Arabian Shield since ~16 Ma from paleo-landforms remnants (Delaunay et al., 2024, submitted in this issue) fall within the same order of magnitude as accumulation in the sink, including the decrease during the Plio-Quaternary (Fig. 9B). This fairly balanced accumulation/denudation budget supports the paleo-drainage reconstructions proposed by Delaunay et al. (2024, submitted in this issue) (Fig. 9C).

Nonetheless, although within the same trend and order of magnitude, estimated denudated volumes are lower than accumulated volumes, particularly in the southern segment (Fig. 9B). This could be related to the fact that the area used to estimate the denudation by Delaunay et al. (2024, submitted in this issue) is missing about 40% of the rifted margin drainage area, in the southern segment. Also, the post-rift accumulation include remobilized evaporites, which makes the estimation of the siliciclastic fraction difficult to evaluate for this time interval and may have induced an overestimation.

5.2. Evolution of sediment routing systems

5.2.1. Contrasting paleogeography during rifting (28–16 Ma)

The acceleration of crustal thinning during the Middle Miocene was associated with marine flooding north of the Yanbu Basin (Fig. 7). The limitation of the marine flooding to the north while the rest of the segment remained continental is consistent with the rift segmentation and the southern magma-rich segment thermally sustained by the influence of the East African hotspot (Baby et al., 2024, submitted). The rift-related relief is not preserved on the coastal plain of the ERSRM and this therefore limits the reconstruction of paleo-drainages. Nonetheless, during rifting in magma-poor settings, the main drainage divides are expected to be located on the uplands associated with the footwalls of the main seaward-dipping, basin-bounding normal faults (e.g., Gawthorpe and Leeder, 2000). Therefore, along the northern segment, the main divides were most probably located along the major normal faults delineating the coastal basins (Fig. 10). Along the magma-rich southern segment, the absence of coarse sediments and bounding faults along the Tihama coastal plain suggests the absence of significant relief during rifting. A recent study of the conjugated rifted margins of South Yemen and Afar (Chauvet et al., 2023) suggested the presence of a central crustal block located along the rift axis of the southern segment, compatible with the geometries observed in this study. According to the model of Geoffroy et al. (2015), this central block (i.e. C-Block) may have acted as a drainage divide at the onset of the rift before being progressively stretched and dismantled as lithosphere thinning increased (Fig. 10).

5.2.2. Drainage reorganization at the ocean-continent transition (16–13 Ma)

At the end of the rifting, the tectonic and magmatic activity decreased in the inner part of the necking domain and the entire rifted margin was flooded by the sea (Fig. 7). The onset of evaporite deposition at the same time (Fig. 4) indicates restricted marine conditions. These changes in accommodation and paleoenvironments were coeval with the regional geodynamic reorganization that led to the oceanisation in the Red Sea, the abandonment of the Suez Rift, and the initiation of the Aqaba and Dead Sea strike-slip fault system (e.g., Bosworth et al., 2005; Courtillot et al., 1987; Delaunay et al., 2023). As previously suggested (e.g, Bosworth et al., 2005; Perrin et al., 1998), this geodynamic event, would have limited the connection between the Red Sea-Gulf of Suez rift system and the Neothetys. Our data do not support the connection with the Indian Ocean at that time suggested by Hughes and Beydoun (1992); Hughes et al. (1991).

At the scale of the rifted margin, the onset of the oceanisation was probably accompanied by the uplift of two portions of the rifted margin that altered the drainage system. First, to the north, (Bayer et al., 1988; Tubbs et al., 2014) documented the inversion of the Midyan half-graben during the activation of the Aqaba-Dead Sea strike-slip fault. This probably induced a new drainage divide oblique to the rift axis following the strike-slip fault. As shown in this study, the coastal plain of the

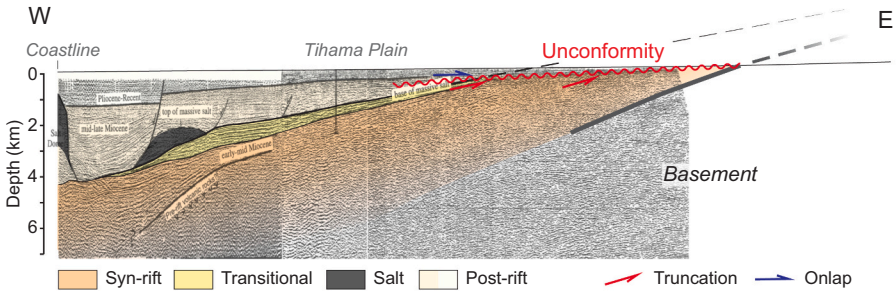

Fig. 9. Interpreted seismic profile illustrating the seaward tilting of the coastal plain along the southern segment of the ERSRM during the post-rift period. Seismic profile and initial interpretation from Davison et al. (1994). The profile was depth converted using a velocity of 3500 m/s. See location on Fig. 2D.

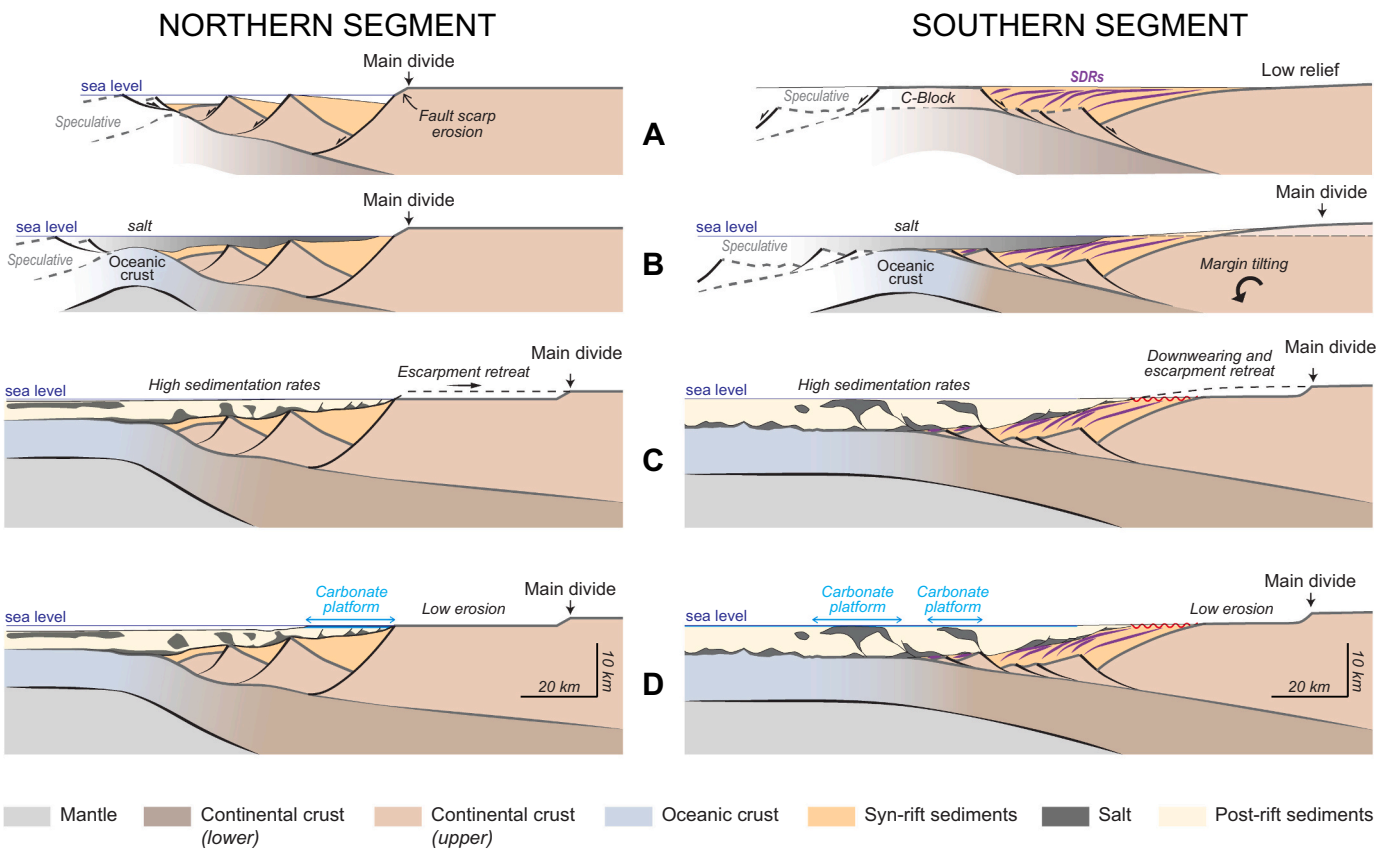

Fig. 10. Schematic cross-sections illustrating the evolution of the sediment routing system for the northern and southern segments of the ERSRM. Original sections from Baby et al. (2024, submitted). (A) Syn-rift (~28–16 Ma). (B) Onset of oceanic crust accretion (~14–13 Ma). (C) Early post-rift (~13–5 Ma). (D) Late post-rift (~5–0 Ma).

southern segment underwent a second uplift (Fig. 10B). This uplift is clearly evidenced by the seismic geometries below the coastal plain (Fig. 9). It was also documented by low-temperature thermochronology data suggesting a Middle Miocene age (~13 Ma) (Turab et al., 2023). According to Stuwe et al. (2022) and Turab et al. (2023), this uplift is linked to the first oceanic crust emplacement which induced a flexural response of the rift shoulders. However, this hypothesis does not explain why the uplift is limited to the southern segment of the margin, as the oceanic accretion in the Red Sea developed along its entire length simultaneously (Augustin et al., 2021; Delaunay et al., 2023) and not only to the south as was previously assumed (Bosworth et al., 2005). Further investigations are needed to better constrain the mechanisms of this post-rift uplift.

5.2.3. *Massive export of solid sediments during the early post-rift (13–5 Ma)*

The precipitation of a thick and massive layer of evaporites marks the onset of the post-rift period in the basin. This evaporite layer acted as a major detachment that strongly influenced the geometry of the post-rift deposits. Accumulated volumes and accumulation rates suggest a massive increase of siliciclastic sediment export (Fig. 8). In the northern segment of the rifted margin, this can be attributed to the retreat of the rift escarpment from ~16 Ma onward that was locally combined with the capture of the endorheic Hamd-Jizl Basin shown by Delaunay et al. (2024, submitted in this issue) (Figs. 8 and 10). Along the southern segment, our observations suggest that the erosion of the coastal plain was triggered by its post-rift uplift. The effective elastic thickness of the lithosphere is expected to be lower in the south than in the north because of the higher thermal gradient related to influence of the East-African and Afar hotspots. Therefore, the flexural response to denudation unloading induced by the escarpment retreat may have been stronger in the south of the margin and have been sustained until the present day. This might explain the difference of morphology with a higher topography and better preservation with respect to the northern segment Delaunay et al. (2024, submitted in this issue) (Fig. 1). However, we cannot rule out the possibility suggested by Stuwe et al. (2022) that climate played a role in the relief of the escarpment. A short period (~7 and 5 Ma) of increase in siliciclastic accumulation was previously documented by Griffin (1999) who attributed it to a major short-lived humidification of the climate during the Messinian (the "Zeit Wet Phase"). According to our study, the duration of this period would be longer (i.e. 14 to 5 Ma), ruling out the existence of a humid event that would be restricted to the Messinian in northeast Africa.

5.2.4. *An aridification of northeast Africa and Arabia in the Pliocene?*

During the late post-rift evolution of the rifted margin (5–0 Ma), accumulated volumes and accumulation rates decreased (Fig. 8) and the rifted margin was dominated by carbonate sedimentation suggesting a very limited denudation of the continent at the time (Fig. 10). Despite the lack of long-term paleoclimatic constraints in the Red Sea, multi-proxy geochemical analysis of marine sediments from Deep Sea Drilling Project site 231 in the Gulf of Aden suggests that Northeast Africa experienced cooling and drying during the Pliocene (Liddy et al., 2016). We therefore propose that this period of low terrigenous fluxes potentially reflects an aridification of northeast Africa and Arabia. This deceleration in erosion of the continent has also been documented by Delaunay et al. (2024, submitted in this issue) onshore and seems to be associated with a slowing (halt?) of the retreat of the margin escarpment (Fig. 10).

Fleisher (1974) showed a contribution of Indian Ocean waters to biogenic carbonate production in the Red Sea sediments since the early Pliocene (Fig. 7). This suggests that, in addition to the climate, the

renewal of carbonate production may well have been related to a restoration of normal salinity conditions when the Red Sea connected to the global ocean. This deconfinement of the basin could have resulted from the propagation of oceanic accretion at the tip of the Gulf of Aden since ~4 Ma (e.g., Manighetti et al., 1997).

5.3. Rift inheritance in the present-day morphology of the carbonate platforms

The northern segment shows a narrow continental shelf (Fig. 1), build-up by aggrading Pliocene to Quaternary carbonate platforms (Fig. 5C). The detailed mapping of these platforms clearly shows that they are located above half-grabens from the proximal necking domain of the margin. The south-western edge of these structures (footwall margin) may have formed a paleo-topographic step that separated the present-day continental shelf with aggrading carbonate platforms from the deep basin (Figs. 2C and 7). In contrast, along the southern segment, the continental shelf is flat and wider, with carbonate platforms all the way to the central oceanic trough (Figs. 2D, 5D, and 7) (Sakellariou et al., 2019). Recent studies in the Red Sea have documented interactions between evaporite withdrawal and the growth of the modern carbonate platforms (Petrovic et al., 2023; Smith and Santamarina, 2022). Our observations suggest a first-order structural control of the segmentation of the rift on the morphology of the platforms. The landward-tilted blocks of the magma-poor northern segment controlled the growth of carbonate platforms in the middle Miocene (i.e. Wadi Waqb Member – Fig. 6A) that developed on the footwall margins (i.e. fault-block platforms) (Bosence, 2012). During the Pliocene – Quaternary, carbonate platform aggradation was controlled by the paleo-topography induced by the proximal tilted blocks. Conversely, the inherited low-relief topography in the necking domain of the magmatic southern segment prevented the development of carbonate platforms during the middle Miocene. The modern platforms seem to be primarily controlled by salt diapirs (Fig. 5E) (Almalki et al., 2015; Davison et al., 1996). Interestingly, the morphology of the African conjugate rifted margin is similar, with a southward widening continental shelf, suggesting a similar structural pattern and rift symmetry (Fig. 1).

6. Conclusions

We investigated the evolution of the sedimentary routing systems of the eastern Red Sea rifted margin by 1) carrying out a reevaluation of the stratigraphic and crustal architecture of the basin, 2) building paleo-environmental maps, and 3) establishing a siliciclastic sediment budget.

- The margin was segmented during the rifting phase (28–16 Ma) between a northern segment, in marine or transitional environments associated with an elevated continental relief (i.e. rift shoulders bounded by major normal faults) and a magmatic southern segment, in continental environments associated with low continental relief.

- The transition phase (16–14 Ma) was accompanied by a marine flooding of the entire basin and the restriction of depositional environments, as evidenced by evaporite precipitation, following a (partial?) disconnection with the open ocean to the north (i.e. Neothetys). Along the southern segment, the coastal plain domain was uplifted and tilted seaward probably during the first oceanic crust emplacement (~14–13 Ma).

- The early post-rift phase of the rifted margin (13–5 Ma) is characterized by a significant increase in the volumes and rates of exported siliciclastic sediments (i.e. 15 times greater than previously deposited volumes), suggesting a rapid erosion of the rift-related relief.

- The late post-rift phase of the rifted margin (5–0 Ma) is marked by a drop in siliciclastic sediment volumes and rates, and a return of carbonate sedimentation, which may indicate an aridification of the climate and a slowdown in the retreat of the onshore escarpment.

Overall, these observations suggest that the contrasting continental relief of the rifted margin, with a higher escarpment to the south, is controlled to first-order by its crustal segmentation and the post-rift uplift of the southern segment. This segmentation is also expressed in the morphology of the margin's present-day carbonate platforms.

CRediT authorship contribution statement

Guillaume Baby: Investigation, Conceptualization, Methodology, Writing – original draft. **Antoine Delaunay:** Investigation, Validation, Writing – review & editing. **Delphine Rouby:** Validation, Methodology, Writing – review & editing. **Jing Ye:** Investigation, Writing – review & editing. **Tihana Pensa:** Investigation, Writing – review & editing. **Abdulkader M. Afifi:** Project administration, Funding acquisition, Investigation, Writing – review & editing.

Declaration of competing interest

The authors declare that they have no known competing financial interests or personal relationships that could have appeared to influence the work reported in this paper.

Data availability

The data that has been used is confidential.

Acknowledgments

This study was completed under KAUST's Competitive Research Grant 4082 on "Geologic Evolution of the Red Sea and Gulf of Aqaba" leaded by Professor Abdulkader M. Afifi. Petroleum companies operating in the Red Sea are acknowledged for the opportunity to interpret their data for scientific purposes. We would also like to thank Julien Bailleul for inviting us to participate in this special issue and two anonymous reviewers for their constructive comments, which helped to improve the quality of our manuscript.

Appendix A. Supplementary data

Supplementary data to this article can be found online at https://doi.org/10.1016/j.earscirev.2024.104679.

References

Afifi, A.M., Tapponnier, P., Raterman, N.S., 2014. The Messinian Unconformity in the Red Sea: Evidence for Widespread Dessication?, 11th Middle east geosciences conference and exhibition. AAPG Search and Discovery Article, Manama, Bahrain, pp. 10–12.

Ahmed, A., Tiberi, C., Leroy, S., Stuart, G.W., Keir, D., Sholan, J., Khanbari, K., Al-Ganad, I., Basuyau, C., 2013. Crustal structure of the rifted volcanic margins and uplifted plateau of Western Yemen from receiver function analysis. Geophys. J. Int. 193 (3), 1673–1690.

Al-Damegh, K., Sandvol, E., Barazangi, M., 2005. Crustal structure of the Arabian plate: New constraints from the analysis of teleseismic receiver functions. Earth Planet. Sci. Lett. 231 (3–4), 177–196.

Ali, M., Decarlis, A., Ligi, M., Ball, P., Bosworth, B., Ceriani, A., 2023. Red Sea rifting in central Egypt: constraints from the offshore Quseir province. J. Geol. Soc. Lond. 180 (2) jgs2022-105.

Almalki, K.A., Ailleres, L., Betts, P.G., Bantan, R.A., 2015. Evidence for and relationship between recent distributed extension and halokinesis in the Farasan Islands, southern Red Sea, Saudi Arabia. Arab. J. Geosci. 8 (10), 8753–8766.

Al-Shanti, A.M.S., 1966. Oolithic iron ore deposits in Wadi Fatima between Jeddah and Mecca, Saudi Arabia. Bull. Saudi Arabian Directorate General Min. Resourc. 2, 51.

Augustin, N., Van Der Zwan, F.M., Devey, C.W., Brandsdóttir, B., 2021. 13 million years of seafloor spreading throughout the Red Sea Basin. Nat. Commun. 12 (1), 2427.

Avni, Y., Segev, A., Ginat, H., 2012. Oligocene regional denudation of the northern Afar dome: Pre- and syn-breakup stages of the Afro-Arabian plate. Geol. Soc. Am. Bull. 124 (11–12), 1871–1897.

Baby, G., Guillocheau, F., Boulogne, C., Robin, C., Dall'Asta, M., 2018. Uplift history of a transform continental margin revealed by the stratigraphic record: the case of the Agulhas transform margin along the Southern African Plateau. Tectonophysics 731, 104–130.

Baby, G., Guillocheau, F., Braun, J., Robin, C., Dall'Asta, M., 2020. Solid sedimentation rates history of the Southern African continental margins: Implications for the uplift history of the South African Plateau. Terra Nova 32 (1), 53–65.

Baby, G., Delaunay, A., Aslanian, D., Afifi, A.M., 2024. Tectonostratigraphic latitudinal evolution of the eastern Red Sea margin. Submitted to BSGF: Earth Sci.
Balestrieri, M.L., Stuart, F.M., Persano, C., Abbate, E., Bigazzi, G., 2005. Geomorphic development of the escarpment of the Eritrean margin, southern Red Sea from combined apatite fission-track and (U-Th)/He thermochronometry. Earth Planet. Sci. Lett. 231 (1–2), 97–110.
Bayer, H.J., Hotzl, H., Jado, A.R., Roscher, B., Voggenreiter, W., 1988. Sedimentary and structural evolution of the Northwest Arabian Red Sea Margin. Tectonophysics 153 (1–4), 137–151.
Bellahsen, N., Faccenna, C., Funiciello, F., Daniel, J.M., Jolivet, L., 2003. Why did Arabia separate from Africa? Insights from 3-D laboratory experiments. Earth Planet. Sci. Lett. 216 (3), 365–381.
Bohannon, R.G., Naeser, C.W., Schmidt, D.L., Zimmermann, R.A., 1989. The timing of uplift, volcanism, and rifting peripheral to the Red Sea: a case for passive rifting? J. Geophys. Res. 94 (B2), 1683–1701.
Bosence, D.W.J., 2012. Carbonate-dominated marine rifts. In: Roberts, D.G., Bally, A.W. (Eds.), Phanerozoic Rift Systems and Sedimentary Basins. Elsevier, Amsterdam, pp. 89–114.
Bosworth, W., 2015. Geological evolution of the Red Sea: historical background, review, and synthesis. In: Rasul, N.M.A., Stewart, I.C.F. (Eds.), The Red Sea: The Formation, Morphology, Oceanography and Environment of a Young Ocean Basin. Springer, Berlin Heidelberg, Berlin, Heidelberg, pp. 45–78.
Bosworth, W., Stockli, D.F., 2016. Early magmatism in the greater Red Sea rift: timing and significance. Can. J. Earth Sci. 53 (11), 1158–1176.
Bosworth, W., Huchon, P., McClay, K., 2005. The Red Sea and Gulf of Aden basins. J. Afr. Earth Sci. 43 (1–3), 334–378.
Braun, J., Beaumont, C., 1989. A physical explanation of the relation between flank uplifts and the breakup unconformity at rifted continental margins. Geology 17 (8), 760–764.
Braun, J., Guillocheau, F., Robin, C., Baby, G., Jelsma, H., 2014. Rapid erosion of the Southern African Plateau as it climbs over a mantle superswell. J. Geophys. Res. Solid Earth 119 (7), 6093–6112.
Burke, K., Gunnell, Y., 2008. The African erosion surface: a continental-scale synthesis of geomorphology, tectonics, and environmental change over the past 180 million years. Geol. Soc. Am. 1–66.
Camp, V.E., Roobol, M.J., 1992. Upwelling asthenosphere beneath Western Arabia and its regional implications. J. Geophys. Res. Solid Earth 97 (B11), 15255–15271.
Chaboureau, A.C., Guillocheau, F., Robin, C., Rohais, S., Moulin, M., Aslanian, D., 2013. Paleogeographic evolution of the central segment of the South Atlantic during Early Cretaceous times: paleotopographic and geodynamic implications. Tectonophysics 604, 191–223.
Chauvet, F., Geoffroy, L., Le Gall, B., Jaud, M., 2023. Volcanic passive margins and break-up processes in the southern Red Sea. Gondwana Res. 117, 169–193.
Cochran, J.R., 2005. Northern Red Sea: Nucleation of an oceanic spreading center within a continental rift. Geochem. Geophys. Geosyst. 6 (3).
Courtillot, V., Armijo, R., Tapponnier, P., 1987. The Sinai Triple Junction Revisited. Tectonophysics 141 (1–3), 181–190.
Davison, I., Alkadasi, M., Alkhirbash, S., Alsubbary, A.K., Baker, J., Blakey, S., Bosence, D., Dart, C., Heaton, R., McClay, K., Menzies, M., Nichols, G., Owen, L., Yelland, A., 1994. Geological Evolution of the Southeastern Red-Sea Rift Margin, Republic of Yemen. Geol. Soc. Am. Bull. 106 (11), 1474–1493.
Davison, I., Bosence, D., Alsop, G.I., Al-Aawah, M.H., 1996. Deformation and sedimentation around active Miocene salt diapirs on the Tihama Plain, Northwest Yemen. Geol. Soc. Lond. Spec. Publ. 100 (1), 23–39.
Davison, I., Tatnell, M.R., Owen, L.A., Jenkins, G., Baker, J., 1998. Tectonic geomorphology and rates of crustal processes along the Red Sea margin, north-West Yemen. In: Purser, B.H., Bosence, D.W.J. (Eds.), Sedimentation and Tectonics in Rift Basins: Red Sea - Gulf of Aden. Springer, Dordrecht, pp. 595–612.
Delaunay, A., Baby, G., Fedorik, J., Afifi, A.M., Tapponnier, P., Dyment, J., 2023. Structure and morphology of the Red Sea, from the mid-ocean ridge to the ocean-continent boundary. Tectonophysics 849, 229728.
Delaunay, A., Baby, G., Garcia Paredes, E., Fedorik, J., Afifi, A.M., 2024. Evolution of the high-elevation eastern Red Sea rifted margin: morphology, uplift processes, and source-to-sink dynamics. Submitted to Earth Sci. Rev.
Doornenbal, J.C., DeGroot, P.F.L., Saif, S.M., Schroot, B.M., 1991. Geology and hydrocarbon potential of the Tihama Basin, Republic of Yemen. Middle East Oil Show, OnePetro, Bahrain.
Dullo, W.-C., Hötzl, H., Jado, A.R., 1983. New stratigraphical results from the Tertiary sequence of the Midyan area, NW Saudi Arabia. Newsl. Stratigr. 12 (2), 75–83.
Egloff, F., Rihm, R., Makris, J., Izzeldin, Y.A., Bobsien, M., Meier, K., Junge, P., Noman, T., Warsi, W., 1991. Contrasting structural styles of the eastern and western margins of the southern Red Sea: the 1988 SONNE experiment. Tectonophysics 198 (2–4), 329–353.
Fedorik, J., Delaunay, A., Losi, G., Panara, Y., Menegoni, N., Afifi, A.M., Arkadakskiy, S., Al Malallah, M., Oelkers, E., Gislason, S.R., Ahmed, Z., Kunnummal, N., 2023. Structure and fracture characterization of the Jizan group: Implications for subsurface CO2 basalt mineralization. Front. Earth Sci. 10.
Fleisher, R.L., 1974. Preliminary report on late neogene Red Sea Foraminifera, deep sea drilling project, Leg, p. 23B.
Gaulier, J.M., Lepichon, X., Lyberis, N., Avedik, F., Geli, L., Moretti, I., Deschamps, A., Hafez, S., 1988. Seismic study of the crust of the northern Red Sea and Gulf of Suez. Tectonophysics 153 (1–4), 55–88.
Gawthorpe, R.L., Leeder, M.R., 2000. Tectono-sedimentary evolution of active extensional basins. Basin Res. 12 (3–4), 195–218.
Geoffroy, L., Burov, E.B., Werner, P., 2015. Volcanic passive margins: another way to break up continents. Sci. Rep. 5 (1), 1–12.
Gilchrist, A.R., Summerfield, M.A., 1990. Differential denudation and flexural isostasy in formation of rifted-margin upwarps. Nature 346 (6286), 739–742.
Gillman, M., 1968. Primary Results of a Geological and Geophysical Reconnaissance of the Jizan Coastal Plain in Saudi Arabia. Regional Technical Symposium, OnePetro, Dahran, Saudi Arabia.
Griffin, D.L., 1999. The late Miocene climate of northeastern Africa: unravelling the signals in the sedimentary succession. J. Geol. Soc. Lond. 156 (4), 817–826.
Guan, H.X., Geoffroy, L., Xu, M., 2021. Magma-assisted fragmentation of Pangea: Continental breakup initiation and propagation. Gondwana Res. 96, 56–75.
Guillocheau, F., Rouby, D., Robin, C., Helm, C., Rolland, N., Carlier, Le, de Veslud, C., Braun, J., 2012. Quantification and causes of the terrigeneous sediment budget at the scale of a continental margin: a new method applied to the Namibia-South Africa margin. Basin Res. 24 (1), 3–30.
Hansen, S.E., Rodgers, A.J., Schwartz, S.Y., Al-Amri, A.M.S., 2007. Imaging ruptured lithosphere beneath the Red Sea and Arabian Peninsula. Earth Planet. Sci. Lett. 259 (3–4), 256–265.
Heaton, R.C., Jackson, M.P.A., Bamahmoud, M., Nani, A.S.O., 1995. Superposed Neogene extension, contraction, and salt canopy emplacement in the Yemeni Red Sea. In: Jackson, M.P.A., Roberts, D.G., Snelson, S. (Eds.), Salt tectonics: a global perspective: AAPG Memoir 65. The American Association of Petroleum Geologists, pp. 333–351.
Hosny, A., Nyblade, A., 2016. The crustal structure of Egypt and the northern Red Sea region. Tectonophysics 687, 257–267.
Hughes, G.W., 2014. Micropalaeontology and palaeoenvironments of the Miocene Wadi Waqb carbonate of the northern Saudi Arabian Red Sea. Geoarabia 19 (4), 59–108.
Hughes, G.W., Beydoun, Z.R., 1992. The Red Sea — Gulf of Aden: biostratigraphy, lithostratigraphy and palaeoenvironments. J. Pet. Geol. 15 (s3), 135–156.
Hughes, G.W., Johnson, R.S., 2005. Lithostratigraphy of the Red Sea region. Geoarabia 10 (3), 49–126.
Hughes, G.W., Varol, O., 2021. Biostratigraphically constrained Neogene palaeoenvironments of the Red Sea rift, The 23rd EGU General Assembly, Vienna, Austria. EGU21-6227.
Hughes, G.W., Varol, O., Beydoun, Z.R., 1991. Evidence for Middle Oligocene rifting of the Gulf of Aden and for late Oligocene rifting of the southern Red-Sea. Mar. Pet. Geol. 8 (3), 354–358.
Hughes, G.W., Grainger, D.J., Abu-Bshait, A.-J., Abdul-Rahman, M.J., 1999. Lithostratigraphy and depositional history of part of the Midyan Region, Northwestern Saudi Arabia. GeoArabia 4 (4), 503–542.
Izzeldin, A.Y., 1987. Seismic, gravity and magnetic surveys in the central part of the Red Sea: their interpretation and implications for the structure and evolution of the Red Sea. Tectonophysics 143 (4), 269–306.
Japsen, P., Bonow, J.M., Green, P.F., Chalmers, J.A., Lidmar-Bergstrom, K., 2006. Elevated, passive continental margins: long-term highs or neogene uplifts? New evidence from West Greenland. Earth Planet. Sci. Lett. 248 (1–2), 330–339.
Kellogg, K.S., Blank, H.R., 1982. Paleomagnetic evidence bearing on Tertiary tectonics of the Tihamat Asir coastal plain, southwestern Saudi Arabia, pp. 82–1047.
Koeshidayatullah, A., Al-Ramadan, K., Collier, R., Hughes, G.W., 2016. Variations in architecture and cyclicity in fault-bounded carbonate platforms: early Miocene Red Sea Rift, NW Saudi Arabia. Mar. Pet. Geol. 70, 77–92.
Kooi, H., Beaumont, C., 1994. Escarpment evolution on high-elevation rifted margins: Insights derived from a surface processes model that combines diffusion, advection, and reaction. J. Geophys. Res. Solid Earth 99 (B6), 12191–12209.
Laspatzis, S., Rouby, D., Rohais, S., Nardin, É., 2023. Meta-analysis of the long-term stratigraphic evolution of rifted margin basins: the GeoDyNamical Analysis approach applied to the South Atlantic Ocean. Basin Res. 35 (3), 898–931.
Le Pichon, X., Gaulier, J.M., 1988. The rotation of Arabia and the Levant fault system. Tectonophysics 153 (1), 271–294.
Leroy, S., Razin, P., Autin, J., Bache, F., d'Acremont, E., Watremez, L., Robinet, J., Baurion, C., Denèle, Y., Bellahsen, N., Lucazeau, F., Rolandone, F., Rouzo, S., Kiel, J. S., Robin, C., Guillocheau, F., Tiberi, C., Basuyau, C., Beslier, M.-O., Ebinger, C., Stuart, G.W., Ahmed, A., Khanbari, K., Al-Ganad, I., de Clarens, P., Unternehr, P., Al-Toubi, K., Al-Lazki, A., 2013. From rifting to oceanic spreading in the Gulf of Aden: A synthesis. In: Al-Hosani, K., Roure, F., Ellison, R., Lokier, S. (Eds.), Lithosphere Dynamics and Sedimentary Basins: The Arabian Plate and Analogues. Frontiers in Earth Sciences. Springer, pp. 385–427.
Liddy, H.M., Feakins, S.J., Tierney, J.E., 2016. Cooling and drying in Northeast Africa across the Pliocene. Earth Planet. Sci. Lett. 449, 430–438.
Manighetti, I., Tapponnier, P., Courtillot, V., Gruszow, S., Gillot, P.-Y., 1997. Propagation of rifting along the Arabia-Somalia plate boundary: the Gulfs of Aden and Tadjoura. J. Geophys. Res. Solid Earth 102 (B2), 2681–2710.
McClusky, S., Reilinger, R., Ogubazghi, G., Amleson, A., Healeb, B., Vernant, P., Sholan, J., Fisseha, S., Asfaw, L., Bendick, R., Kogan, L., 2010. Kinematics of the southern Red Sea-Afar Triple Junction and implications for plate dynamics. Geophys. Res. Lett. 37 (5).
Menzies, M.A., Baker, J., Bosence, D., Dart, C., Davison, I., Hurford, A., Al'Kadasi, M., McClay, K., Nichols, G., Al'Subbary, A., Yelland, A., 1992. The timing of magmatism, uplift and crustal extension: preliminary observations from Yemen. Geol. Soc. Lond. Spec. Publ. 68 (1), 293–304.
Menzies, M.A., Gallagher, K., Yelland, A., Hurford, A.J., 1997. Volcanic and nonvolcanic rifted margins of the Red Sea and Gulf of Aden: crustal cooling and margin evolution in Yemen. Geochim. Cosmochim. Acta 61 (12), 2511–2527.
Mitchell, N.C., Shi, W., Izzeldin, A.Y., Stewart, I.C.F., 2021. Reconstructing the level of the Central Red Sea evaporites at the end of the Miocene. Basin Res. 33 (2), 1266–1292.

Molnar, N., Cruden, A., Betts, P., 2020. The role of inherited crustal and lithospheric architecture during the evolution of the Red Sea: insights from three dimensional analogue experiments. Earth Planet. Sci. Lett. 544, 116377.
Mooney, W.D., Gettings, M.E., Blank, H.R., Healy, J.H., 1985. Saudi-Arabian seismic-refraction profile: a traveltime interpretation of crustal and upper mantle structure. Tectonophysics 111 (3–4), 173–246.
Moretti, I., Colletta, B., 1987. Spatial and temporal evolution of the Suez Rift subsidence. J. Geodyn. 7 (1–2), 151–168.
Ouf, M.A.A., Gheith, A.M., 1998. Sedimentary evolution of early rift troughs of the Central Red Sea margin, Jeddah, Saudi Arabia. In: Purser, B.H., Bosence, D.W.J. (Eds.), Sedimentation and Tectonics in Rift Basins: Red Sea - Gulf of Aden. Springer, Netherlands, Dordrecht, pp. 135–145.
Partridge, T.C., 1997. Late Neogene uplift in eastern and southern Africa and its paleoclimatic implications. In: Ruddiman, W.F. (Ed.), Tectonic Uplift and Climate Change. Springer, US, Boston, MA, pp. 63–86.
Pensa, T., Afifi, A.M., Delaunay, A., Baby, G., 2022. Tectonic Control on the Reef Evolution in the Red Sea Syn-Rift Basin, the 24th EGU General Assembly, Vienna, Austria.
Pensa, T., Huertas, A.D., Aljahdali, A.H., Afifi, A.M., 2023. Geological Evolution of the Post-Rift Section in the Red Sea Basin, the International Meeting for Applied Geoscience & Energy (IMAGE), Houston, USA.
Perrin, C., Plaziat, J.C., Rosen, B.R., 1998. Miocene coral reefs and reef corals of the South-Western Gulf of Suez and North-Western Red Sea: Distribution, diversity and regional environmental controls. In: Purser, B.H., Bosence, D.W.J. (Eds.), Sedimentation and Tectonics in Rift Basins: Red Sea - Gulf of Aden. Springer, Netherlands, Dordrecht, pp. 296–319.
Petit, C., Fournier, M., Gunnell, Y., 2007. Tectonic and climatic controls on rift escarpments: Erosion and flexural rebound of the Dhofar passive margin (Gulf of Aden, Oman). J. Geophys. Res. Solid Earth 112 (B3).
Petrovic, A., Lüdmann, T., Afifi, A.M., Saitz, Y., Betzler, C., Vahrenkamp, V., 2023. Fragmentation, rafting, and drowning of a carbonate platform margin in a rift-basin setting. Geology 51 (3), 242–246.
Phillips, J.D., Ross, D.A., 1970. A discussion on the structure and evolution of the Red Sea and the nature of the Red Sea, Gulf of Aden and Ethiopia rift junction - Continuous seismic reflexion profiles in the Red Sea. Hilosophical Trans. Royal Soc. London. Ser A Math. Physical Sci. 267, 143–152.
Pindell, J., Graham, R., Horn, B., 2014. Rapid outer marginal collapse at the rift to drift transition of passive margin evolution, with a Gulf of Mexico case study. Basin Res. 26 (6), 701–725.
Reilinger, R., McClusky, S., 2011. Nubia–Arabia–Eurasia plate motions and the dynamics of Mediterranean and Middle East tectonics. Geophys. J. Int. 186 (3), 971–979.
Ribot, M., Klinger, Y., Jonsson, S., Avsar, U., Pons-Branchu, E., Matrau, R., Mallon, F.L., 2021. Active Faults' Geometry in the Gulf of Aqaba, Southern Dead Sea Fault, Illuminated by Multibeam Bathymetric Data. Tectonics 40 (4) e2020TC006443.
Rihm, R., Makris, J., Möller, L., 1991. Seismic surveys in the Northern Red Sea: asymmetric crustal structure. Tectonophysics 198 (2), 279–295.
Rouby, D., Bonnet, S., Guillocheau, F., Gallagher, K., Robin, C., Biancotto, F., Dauteuil, O., Braun, J., 2009. Sediment supply to the Orange sedimentary system over the last 150My: an evaluation from sedimentation/denudation balance. Mar. Pet. Geol. 26 (6), 782–794.
Sakellariou, D., Rousakis, G., Panagiotopoulos, I., Morfis, I., Bailey, G.N., 2019. Geological structure and late quaternary geomorphological evolution of the Farasan Islands Continental Shelf, South Red Sea, SW Saudi Arabia. In: Rasul, N.M.A., Stewart, I.C.F. (Eds.), Geological Setting, Palaeoenvironment and Archaeology of the Red Sea. Springer International Publishing, Cham, pp. 629–652.
Schmidt, D.L., Hadley, D.G., 1985. Stratigraphy of the Miocene Baid Formation, Southern Red Sea Coastal Plain. Kingdom of Saudi Arabia.
Schmidt, D.L., Hadley, D.G., Brown, G.F., 1983. Middle Tertiary Continental Rift and Evolution of the Red Sea in Southwestern Saudi Arabia, Reston, VA.
Sebai, A., Zumbo, V., Feraud, G., Bertrand, H., Hussain, A.G., Giannerini, G., Campredon, R., 1991. $^{40}Ar/^{39}Ar$ dating of alkaline and tholeiitic magmatism of Saudi-Arabia related to the early Red-Sea Rifting. Earth Planet. Sci. Lett. 104 (2–4), 473–487.
Smith, J.E., Santamarina, J.C., 2022. Red Sea evaporites: formation, creep and dissolution. Earth Sci. Rev. 232, 104115.
Stanley, J.R., Braun, J., Baby, G., Guillocheau, F., Robin, C., Flowers, R.M., Brown, R., Wildman, M., Beucher, R., 2021. Constraining Plateau Uplift in Southern Africa by Combining Thermochronology, Sediment Flux, Topography, and Landscape Evolution Modeling. J. Geophys. Res. Solid Earth 126 (7) e2020JB021243.
Stern, R.J., 1985. The Najd Fault System, Saudi Arabia and Egypt: A late Precambrian rift-related transform system? Tectonics 4 (5), 497–511.
Stern, R.J., Johnson, P.R., 2019. Constraining the opening of the Red Sea: evidence from the Neoproterozoic Margins and Cenozoic Magmatism for a Volcanic Rifted Margin. In: Rasul, N.M.A., Stewart, I.C.F. (Eds.), Geological Setting, Palaeoenvironment and Archaeology of the Red Sea. Springer International Publishing, Cham, pp. 53–79.
Sternai, P., Muller, V.A.P., Jolivet, L., Garzanti, E., Corti, G., Pasquero, C., Sembroni, A., Faccenna, C., 2021. Effects of asthenospheric flow and orographic precipitation on continental rifting. Tectonophysics 820, 229120.
Stockli, D.F., Bosworth, W., 2019. Timing of extensional faulting along the Magma-Poor Central and Northern Red Sea Rift Margin—transition from regional extension to necking along a hyperextended rifted margin. In: Rasul, N.M.A., Stewart, I.C.F. (Eds.), Geological Setting, Palaeoenvironment and Archaeology of the Red Sea. Springer International Publishing, Cham, pp. 81–111.
Stuwe, K., Robl, J., Turab, S.A., Sternai, P., Stuart, F.M., 2022. Feedbacks between sea-floor spreading, trade winds and precipitation in the Southern Red Sea. Nat. Commun. 13 (1), 5405.
Szymanski, E., Stockli, D.F., Johnson, P.R., Hager, C., 2016. Thermochronometric evidence for diffuse extension and two-phase rifting within the Central Arabian Margin of the Red Sea Rift. Tectonics 35 (12), 2863–2895.
Tapponnier, P., Dyment, J., Zinger, M.A., Franken, D., Afifi, A.M., Wyllie, A., Ali, H.G., Hanbal, I., 2013. Revisiting seafloor-spreading in the Red Sea: basement nature, transforms and ocean-continent boundary, AGU Fall Meeting Abstracts, pp. T12B–04.
Tubbs, R.E.J., Fouda, H.G.A., Afifi, A.M., Raterman, N.S., Hughes, G.W., Fadolalkarem, Y.K., 2014. Midyan Peninsula, northern Red Sea, Saudi Arabia: Seismic imaging and regional interpretation. Geoarabia 19 (3), 165–184.
Tucker, G.E., Slingerland, R.L., 1994. Erosional dynamics, dlexural isostasy, and long-lived escarpments: a numerical modeling study. J. Geophys. Res. Solid Earth 99 (B6), 12229–12243.
Turab, S.A., Stuwe, K., Stuart, F.M., Cogne, N., Chew, D.M., Robl, J., 2023. A two phase escarpment evolution of the Red Sea margin of southwestern Saudi Arabia. insights from low-temperature apatite thermochronology. Earth Planet. Sci. Lett. 603, 117990.
van der Beek, P., Cloetingh, S., Andriessen, P., 1994. Mechanisms of extensional basin formation and vertical motions at rift flanks: Constraints from tectonic modelling and fission-track thermochronology. Earth Planet. Sci. Lett. 121 (3–4), 417–433.
van der Beek, P., Andriessen, P., Cloetingh, S., 1995. Morphotectonic evolution of rifted continental margins: inferences from a coupled tectonic-surface processes model and fission track thermochronology. Tectonics 14 (2), 406–421.
van der Beek, P., Summerfield, M.A., Braun, J., Brown, R.W., Fleming, A., 2002. Modeling postbreakup landscape development and denudational history across the southeast African (Drakensberg Escarpment) margin. J. Geophys. Res. Solid Earth 107 (B12). ETG 11-1-ETG 11-18.
Vicente de Gouveia, S., Besse, J., Frizon de Lamotte, D., Greff-Lefftz, M., Lescanne, M., Gueydan, F., Leparmentier, F., 2018. Evidence of hotspot paths below Arabia and the Horn of Africa and consequences on the Red Sea opening. Earth Planet. Sci. Lett. 487, 210–220.
Viltres, R., Jonsson, S., Alothman, A.O., Liu, S.Z., Leroy, S., Masson, F., Doubre, C., Reilinger, R., 2022. Present-Day Motion of the Arabian Plate. Tectonics 41 (3) e2021TC007013.
Zalmout, I.S., Sanders, W.J., Maclatchy, L.M., Gunnell, G.F., Al-Mufarreh, Y.A., Ali, M.A., Nasser, A.A., Al-Masari, A.M., Al-Sobhi, S.A., Nadhra, A.O., Matari, A.H., Wilson, J. A., Gingerich, P.D., 2010. New Oligocene primate from Saudi Arabia and the divergence of apes and Old World monkeys. Nature 466 (7304), 360–364.
Ziegler, M.A., 2001. Late Permian to Holocene paleofacies evolution of the Arabian Plate and its hydrocarbon occurrences. GeoArabia 6 (3), 445–504.